PERIODICO di MINERALOGIA
established in 1930

Dipartimento
di Scienze della Terra

Sapienza
Università di Roma

An International Journal of
Mineralogy, Crystallography, Geochemistry,
Ore Deposits, Petrology, Volcanology
and applied topics on Environment, Archaeometry and Cultural Heritage

Fluid inclusion and Pb-O isotope constraints on the genesis of the Jurassic Karaburun VMS deposit (Central Pontides, Türkiye)

Buğra Çavdar [1,2,*], Kurtuluş Günay [1], Halim Mutlu [2], Eren Çantay [3], Elif Ekebaş-Çavdar [3], Emin Çiftçi [4], Amr Abdelnasser [4,5]

[1] Mineral Research and Exploration Department, General Directorate of Mineral Research and Exploration, 06530, Ankara, Türkiye
[2] Department of Geological Engineering, Faculty of Engineering, Ankara University, 06830, Ankara, Türkiye
[3] Turkish Energy, Nuclear and Mineral Research Agency, Nuclear Energy Research Institute, 06980, Ankara, Türkiye
[4] Department of Geological Engineering, Faculty of Mines, İstanbul Technical University, 34469, İstanbul, Türkiye
[5] Geology Department, Faculty of Science, Benha University, 13518, Benha, Egypt

ARTICLE INFO

Submitted: November 2025
Accepted: January 2026
Available on line: March 2026

* Corresponding author:
bugracavdar23@gmail.com

Doi: 10.13133/2239-1002/19139

How to cite this article:
Çavdar B. et al. (2026)
Period. Mineral. 95, 25-50

ABSTRACT

The Jurassic Karaburun deposit of the Central Pontides represents one of the largest known volcanogenic massive sulphide (VMS) systems in Türkiye, comprising ~125 Mt of ore with average grade 1.16 wt% Cu, 0.25 wt% Zn, and 0.05 wt% Co. Mineralization is hosted by low-grade greenschist-facies rocks of the Çangaldağ Metamorphic Complex (CMC), where volcaniclastic and detrital successions interlayered with deep-marine sediments are intruded by mafic dikes and sills. Ore occurs mainly as stratiform, sheet-like to tabular bodies, expressed by disseminated, banded, pyritic clastic, semi-massive, and massive sulphide textures. To constrain ore-fluid evolution and metal provenance, we investigate primary fluid inclusions in ore-stage quartz and combined microthermometry with quartz $\delta^{18}O$ and massive-sulphide Pb isotopes. Two-phase inclusions yield eutectic temperatures of −26 to −11 °C and lack clathrate formation, indicating a dominant H_2O-NaCl system. Homogenization temperatures of 178-301 °C, corrected for ~160 bar hydrostatic pressure, imply trapping at 223±25 °C; ice-melting temperatures correspond to 1.4-11.1 wt% NaCl equiv. (mean 6.5 wt%). Moderately elevated salinity and the absence of boiling features support seawater-derived fluids modified by subseafloor circulation, with limited magmatic input. Quartz $\delta^{18}O$ values (11.79 ‰ to 14.40 ‰ VSMOW) require isotopically evolved fluids, giving $\delta^{18}O_{(fluid)}$ of ~3-6‰ at FI-constrained temperatures. Pb isotope ratios ($^{208}Pb/^{204}Pb$=37.463-37.751; $^{207}Pb/^{204}Pb$=15.424-15.503; $^{206}Pb/^{204}Pb$=18.079-18.431) are weakly radiogenic and narrowly variable, consistent with a predominately mantle-derived Pb source. Collectively, these constraints indicate formation in a Jurassic ensimatic arc-back-arc basin undergoing rifting, with chiefly seawater hydrothermal fluids modestly overprinted by magmatic volatiles.

Keywords: Central Pontides, Karaburun VMS; pelitic-mafic type; Pb-O isotope geochemistry; fluid inclusion.

INTRODUCTION

Volcanogenic massive sulphide (VMS) deposits constitute one of the most enduring and economically significant ore systems on Earth, forming from the Archean to the present day and supplying major proportions of base metals (Cu, Pb, Zn) and precious metals (Ag, Au), in addition to a suite of critical by-products including Co, Sn, In, Cd, Tl, Ga, Se, Ge, Sb and Bi (Franklin et al., 1981; Lydon, 1988). These deposits originate in submarine hydrothermal systems where heated, metal-bearing fluids circulate convectively through permeable volcanic and sedimentary successions beneath seafloor. Ore is typically deposited at, or immediately below, the sediment-water interface, generating lensoid to stratabound/stratiform sulphide accumulations with sharp contacts against their host rocks (Franklin et al., 1981; Eldridge et al., 1983; Herzig and Hannington, 1995; Piercey, 2011; Tornos et al., 2015).

Globally, thousands of VMS deposits have been recognized in tectonic environments characterized by extension and high heat flaw, including mid-ocean ridges, back-arc basins, oceanic arcs, and continental rifts (Cathles, 1983; Lentz, 1998; Barrie and Hannington, 1999; Franklin et al., 2005; Galley et al., 2007; Piercey, 2011). In these settings, volcanism and/or subvolcanic intrusive complexes provide the thermal engine required to sustain high-temperature hydrothermal circulation and extensive subseafloor alteration (Franklin et al., 1981; Cathles, 1983; Galley, 1993, 2003; Piercey et al., 2003). Whether such systems ultimately generate-and preserve-economic sulphide bodies are controlled by the interplay among magmatic heat availability, permeability, longevity of convective circulation, fluid composition, seawater physicochemical conditions, water depth, and depositional environment (Barrie et al., 1997; Doyle and Allen, 2003; Franklin et al., 2005; Monecke et al., 2014; Tornos et al., 2015). Because of their favourable mining characteristics, high grades, polymetallic nature, and well-defined margins, they were among the earliest metallic ore deposits identified and remain exceptionally attractive target for mineral exploration (Franklin et al., 1981, 2005; Slack, 1993; Barrie and Hannington, 1999; Mosier et al., 2009). Major districts and resources are documented across United States of America, Spain, Finland, Norway, Türkiye, the Arabian Peninsula, Russia, Australia, and Japan (Galley et al., 2007; Mosier et al., 2009).

Within the global framework, Anatolia (Asia Minor, Türkiye) is strategically positioned in the central sector of the Tethyan metallogenic belt, an extensive ore-forming domain extending from China to Italy (e.g., Yiğit, 2009; Richards, 2015; Kuşcu et al., 2019). Previous studies have emphasized two principal VMS styles in Türkiye: mafic-type deposits linked to the Southeastern Anatolian Orogenic Belt or Bitlis Zagros Suture Zone (BZSZ), and bimodal felsic-type deposits associated with the Early Campanian-Maastrichtian magmatic arc of the Eastern Pontides (e.g., Çiftçi and Hagni, 2005; Yiğit, 2009; Revan et al., 2013, 2017; Eyüboğlu et al., 2014; Köprübaşı et al., 2014; Yıldırım et al., 2016; Rabayrol et al., 2023; Sönmez et al., 2025). More recent work, supported by intensive exploration and new discoveries in the BZSZ and the Central Pontides, has expanded this classification to include bimodal-mafic (Günay, 2021, 2023; Günay et al., 2022; Özkan et al., 2025) and pelitic-mafic types (Günay et al., 2018, 2019; Yıldırım et al., 2019; Baran et al., 2021; Çavdar and Günay, 2023; Çavdar et al., 2025b). In parallel, the Central Pontides have gained increasing prominence in economic geology following the recognition of multiple VMS occurrences; integrated geological, petrographic, geochemical and geochronological studies collectively indicate that this region represents a distinct metallogenic province (Çakır, 1995; Okay et al., 2006, 2013; Dönmez et al., 2014; Altun et al., 2015; Akbulut et al., 2016; Çelik et al., 2016; Çimen et al., 2016, 2017, 2018; Günay et al., 2016, 2018, 2019, 2022; Frassi et al., 2017; Çiftçi, 2019; Çimen, 2020a, b; Günay, 2021; Baran et al., 2021; Yalçın et al., 2023; Çavdar and Günay, 2023, 2025; Günay, 2023; Günay and Çavdar, 2024; Çavdar et al., 2024, 2025a, b).

The Jurassic Karaburun VMS deposit-among the most recent discoveries in the Central Pontides-forms the focal point of this contribution. During early-stage exploration, stream and soil geochemical datasets provided a decisive vector toward mineralization (Çavdar et al., 2025a). Subsequent detailed investigations established a robust geological and genetic framework, including deposit-scale geology, ore textures, basalt and sulphide geochemistry, geochronological constraints, and ore-forming processes (Çavdar et al., 2025b). On the basis of these datasets and resource estimation, Karaburun has been characterized as a giant pelitic-mafic VMS system containing an inferred resource of 125 Mt @ 1.16 wt% Cu, 0.25 wt% Zn, and 0.05 wt% Co (Günay et al., 2024; Çavdar et al., 2025b). Given its scale and metal endowment, the deposit is of considerable economic value, and mining and operational activities are currently underway.

Despite these advances, key constraints on fluid evolution and metal sourcing remain insufficiently resolved. In particular, systematic fluid inclusion investigations and Pb-O isotope geochemistry have not yet been reported for the Karaburun deposit. Furthermore, other VMS deposits hosted by the Çangaldağ Metamorphic Complex (CMC) have not been assessed through fluid inclusion microthermometry, underscoring the need for regionally consistent datasets. Comparable gaps also exist for Pb-O isotopic characterization of other pelitic-mafic type VMS deposits that share important geological and metallogenic similarities with the Karaburun deposit (i.e., Günay et al., 2018, 2019; Baran et al., 2021). Addressing these limitations, the present study provides the first fluid inclusion and stable isotope constraints on the physicochemical properties of the hydrothermal fluids and the conditions prevailing during sulphide deposition. The resulting interpretations not only refine genetic understanding of the Karaburun system but also offer broader implications for CMC-hosted deposits in the Central Pontides and for analogous VMS systems worldwide.

GEOLOGICAL BACKGROUND

Regional geological setting

Anatolia, a major segment of the Alpine orogeny, was shaped at the end of the Mesozoic through the amalgamation of various microplates and continental fragments that rifted from Laurasia to the south and Gondwana to the north, following the closure of the Neotethys, Paleotethys, or the Intra Pontide oceans (Şengör and Yılmaz, 1981; Ustaömer and Robertson, 1993, 1994, 1999; Okay and Tüysüz, 1999; Okay et al., 2006, 2013, 2014; Göncüoğlu et al., 2014; Marroni et al., 2014, 2020). Three principal tectonic units that constitute this geography are named as the Pontides in the north, the Arabian Platform in the southeast, and the Anatolide-Tauride Block situated between these blocks (Şengör and Yılmaz, 1981; Okay and Tüysüz, 1999; Figure 1a). The Pontides, also including the study area, extend across the region between the İzmir-Ankara-Erzincan suture zone (IAESZ) and the Black Sea. They have been subdivided into three regions-Western, Central, and Eastern-based on their geological, geochemical, geochronological, paleontological, and distinct tectonomagmatic evolutions (Şengör and Yılmaz, 1981; Tüysüz, 1999). The Central Pontides, separated by the Intra-Pontide Suture Zone and composed of Sakarya Zone and the İstanbul-Zonguldak Zone fragments, represents the central northern part of the Pontides (Figure 1a; Okay and Nikishin, 2015; Çimen et al., 2017). Within this framework, the Central Pontides correspond to a geographic designation that comprises units and complexes of diverse origins, either regional, geographic, fundamental or tectonic in nature (Ustaömer and Robertson, 1999; Kozur et al., 2000; Okay et al., 2006, 2013, 2014, 2018; Göncüoğlu et al., 2014; Okay and Nikishin, 2015; Aygül et al., 2016; Sayıt et al., 2016; Çimen et al., 2016, 2017, 2018, 2024; Gücer et al., 2016, 2019; Çimen, 2020a, b; Marroni et al., 2020). The complex forming the southern and central part of the Central Pontides, extending approximately 50 km in length and 40 km in width (Çimen et al., 2016), has been named as the Central Pontides Supercomplex (CPS: Okay et al., 2013) or the Central Pontides Structural Complex (Figure 1a; CPSC: Tekin et al., 2012) The CMC constitutes one of the principal tectonic units of the CPSC, representing the remnants of the Intra Pontide branch of the Neotethys (Figure 1b; Çimen et al., 2016, 2017). The complex comprises a wide range of low-grade metamorphic rocks, including intrusive, extrusive rocks spanning compositions from felsic to mafic, and volcaniclastic rocks, as well as deep-marine sediments (Okay et al., 2013, 2018; Çimen et al., 2016; Günay et al., 2018, 2019, 2022). Radiometric ages, along with the geological, geochemical features and associated tectonomagmatic evolution of the region, indicate that an active intra-oceanic arc system-comprising fore-arc, ensimatic island-arc, and back-arc components-existed at least during the Jurassic (Okay et al., 2013, 2018; Çimen et al., 2016, 2017; Alparslan and Dilek, 2018; Marroni et al., 2020). The geodynamic processes, volcanic activity, and associated hydrothermal circulation within this system were sufficiently favourable to generate various types of VMS deposits during that time.

The CMC consists of two crustal-scale tectonic slices located to the north and south of the Gökırmak fold-and-thrust belt (Figure 1b). Both tectonic slices host several exploited as well as newly discovered VMS deposits. The presence of both bimodal-mafic and pelitic-mafic VMS deposits in the northern and southern parts of the CMC highlights the complex as a significant metallogenic provenance (Figure 1b). The northern section hosts both types of deposits (e.g., Zeybek, Cünür, Say Yayla, Sarıseki, Büyük Hill, Örhen, Cozoğlu; Günay et al., 2019, 2022; Çiftçi, 2019; Baran et al., 2021; Günay, 2021, 2023; Çavdar and Günay, 2025; Özkan et al., 2025). In the southern section, the pelitic-mafic Hanönü VMS deposit (currently being exploited; 24.45 Mt @ 1.64% Cu; Günay et al., 2018), and the giant Karaburun VMS deposit emphasizes the economic significance and potential of the area (Çavdar et al., 2025 a,b). Zircon U-Pb ages from volcanic rocks hosting mineralization, along with Re-Os geochronological data from various deposits in the region, consistently indicate a Middle-Late Jurassic age (Akbulut et al., 2016; Çimen et al., 2018; Günay et al., 2019, 2022; Günay, 2023; Çavdar et al., 2025b). Following their formation, these deposits underwent multiphase deformation and metamorphism at various stages between the Late Cretaceous and Neogene (e.g., Günay et al., 2018, 2019, 2022; Çavdar et al., 2025b). In addition to these, the mafic-type Küre deposits in the region (Çağatay et al., 1980; Güner, 1980; Çağatay, 1993; Koç et al., 1995; Çakır, 1995; Kuşcu and Erler, 2002; Altun et al., 2015; Akbulut et al., 2016), as well as the subeconomic pelitic-mafic VMS deposits such as Gökçedoğan (Yalçın et al., 2022) and Kömürlükdere-Göçükdibi (Yalçın et al., 2023) contribute to the understanding of the regional metallogenic framework.

Deposit geology

The Karaburun VMS deposit (41°53’N, 34°59’E; Sinop Province, Türkiye) occurs within the low-grade greenschist-facies metamorphic rocks of the CMC.

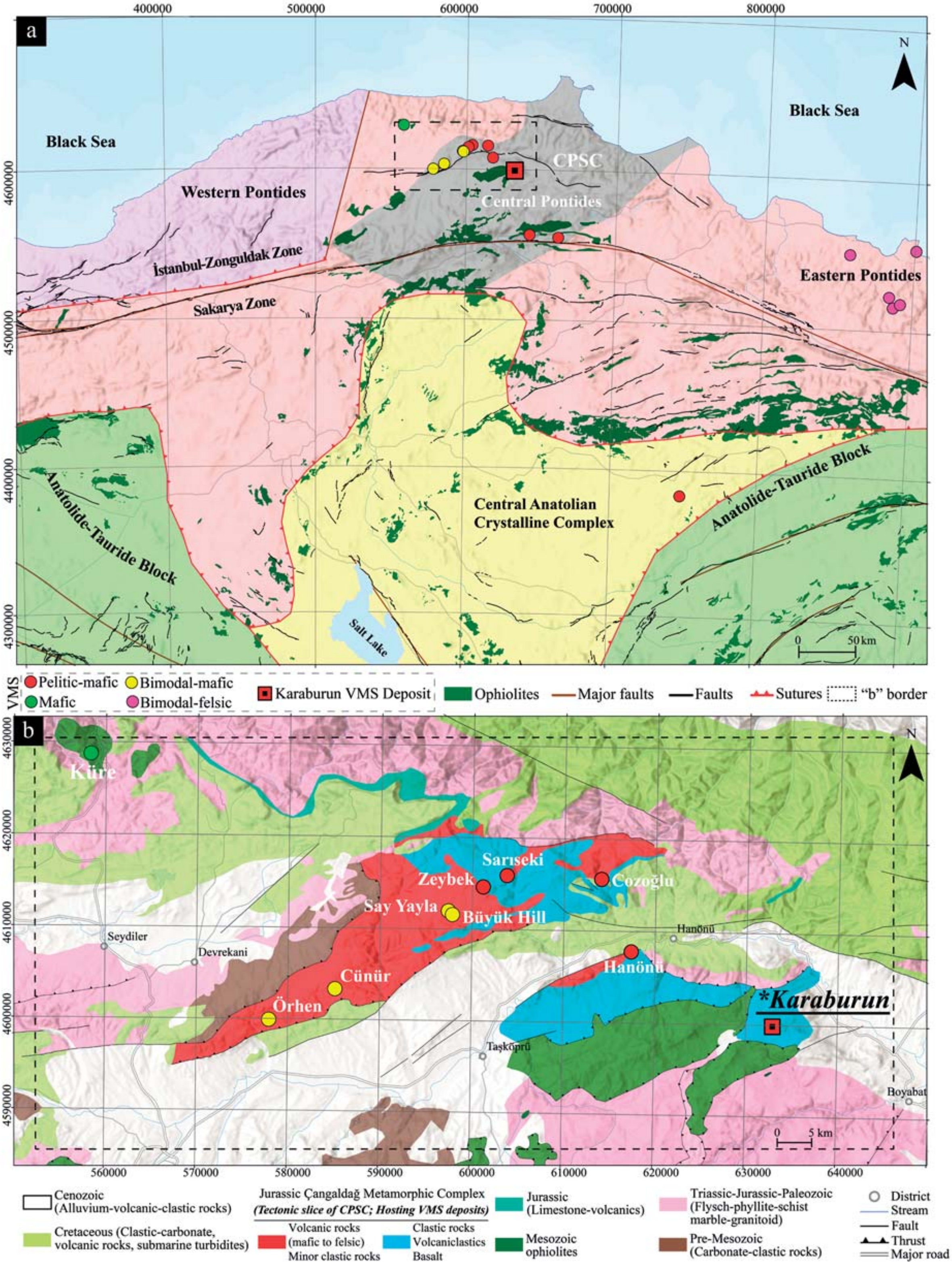

Figure 1. a) The tectonic map showing the major blocks in the central-northern part of Türkiye and the major VMS deposits in the region (Okay and Tüysüz, 1999; Yiğit, 2009; Günay et al., 2018; Kuşcu et al., 2019; Çiftçi, 2019; Marroni et al., 2020); b) simplified geological map of the Central Pontides, showing the VMS deposits in the region (modified after Çimen et al., 2016; Günay et al., 2018, 2019, 2022; Baran et al., 2021; Çavdar et al., 2025b). Abbreviation: CPSC=Central Pontides Structural Complex.

The detailed geological characteristics of the deposit, including host rock associations, structural features, alteration styles, post-mineralization processes and the textural and mineralogical attributes of the deposit, are comprehensively described in Çavdar et al. (2025b). Based on this research, the lithologies associated with the deposit (Re-Os pyrite age: 163.6±7.1) comprise volcaniclastic and clastic detrital sedimentary rocks, deep-marine sediments, and sub-seafloor mafic dikes and/or sills. All units, except for the black shale precursor phyllites, are classified as schist units, as their surface exposures are extremely limited due to dense vegetation cover, and their lateral continuity is therefore difficult to trace in the field (Figure 2). The volcanic rocks are subalkaline to tholeiitic basalts, derived from a depleted MORB-type mantle source enriched by a subduction component, consistent with an intra-oceanic back-arc geodynamic setting. The volcaniclastic rocks are interbedded with the clastic succession and they are predominantly characterized as epidote-chlorite schist, chlorite schist, and quartz-chlorite schist. These units mostly occur in the hanging wall of mineralization and typically exhibit intense epidote (± chlorite ± white mica) alteration (Figure 3a). Chlorite-phyllites are distinguished by green to dark green colours and are composed mainly of chlorite, quartz, muscovite, and minor epidote, displaying lepidoblastic to lepidogranoblastic textures with pervasive chlorite alteration (Figure 3b). Clastic rocks, derived from siltstone-greywacke protoliths, consist predominantly of quartz, muscovite ± chlorite ± epidote ± plagioclase ± carbonate ± pyrite ± magnetite ± hematite minerals. Black shale precursor phyllites are characterized by

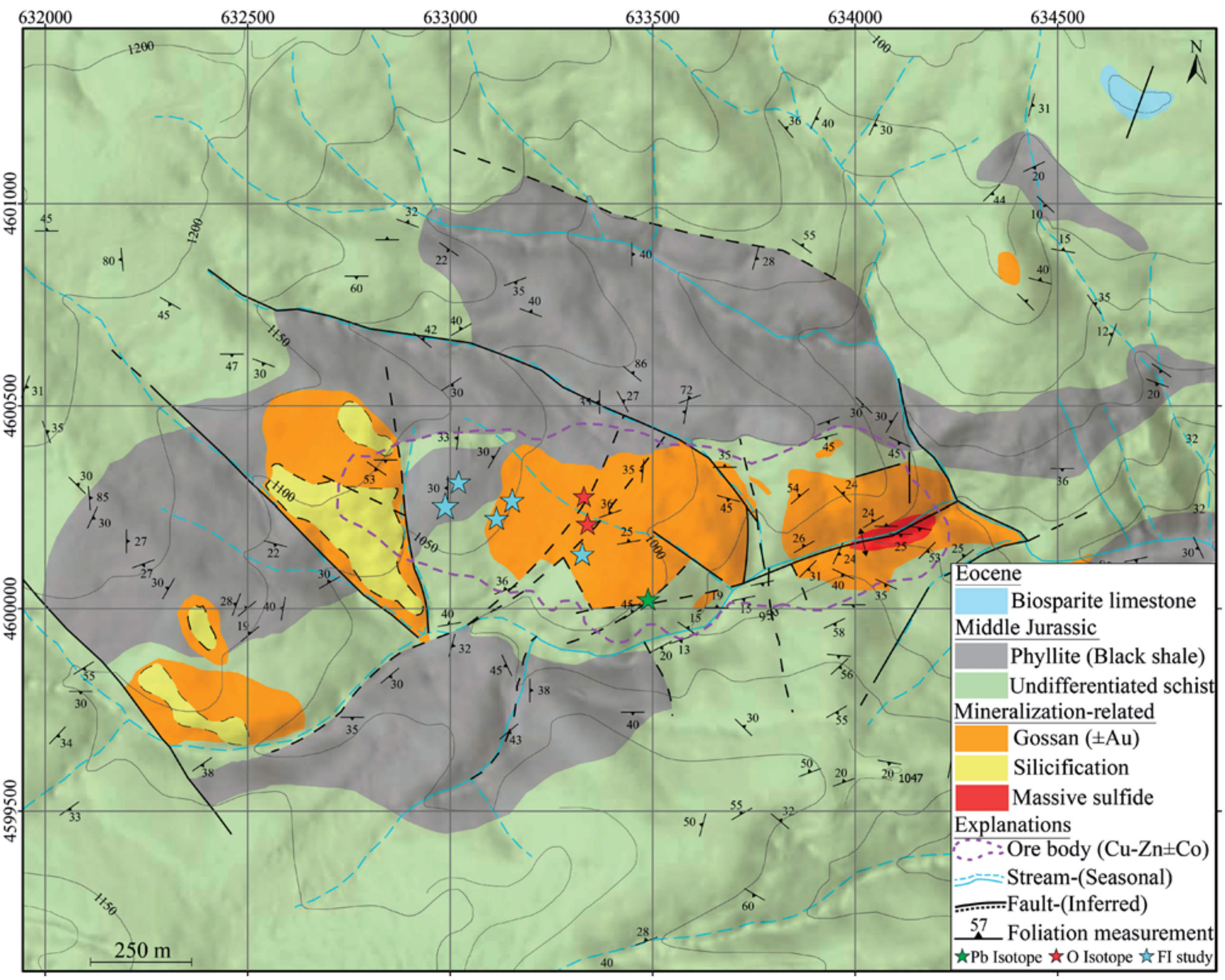

Figure 2. Geological map of the Karaburun VMS deposit, showing the surface projection of the estimated ore body (adapted and modified from Çavdar et al., 2025b). Star symbols in different colours (see the legend) indicate the drillholes from which the corresponding analyses were completed.

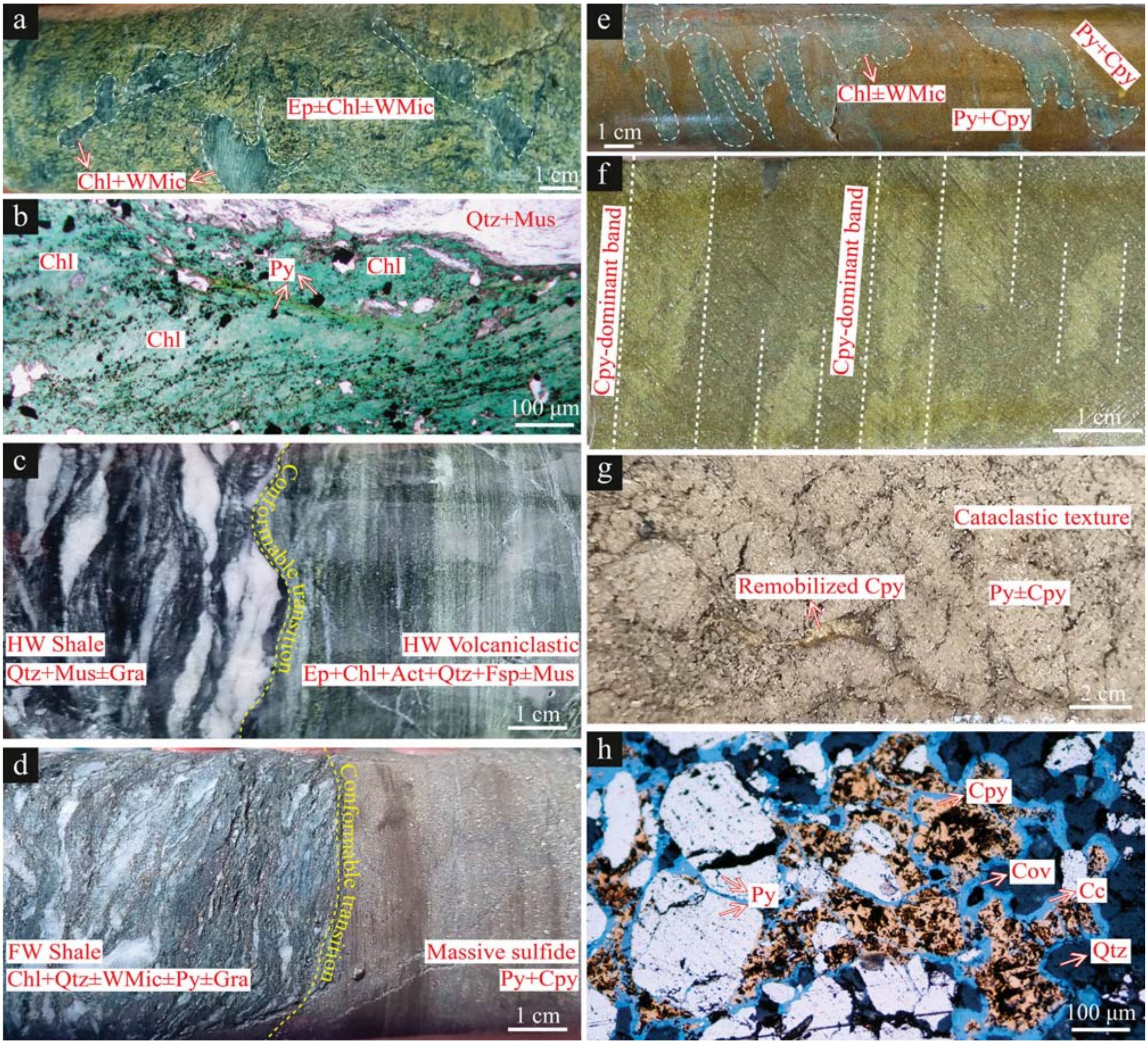

Figure 3. Micro- and macrophotographs from Karaburun mineralization, hydrothermal alteration, wall rocks, textures and supergene enrichment. a) Pervasive epidote alteration in the hanging wall volcaniclastic rocks and chlorite-white mica alteration halos, b) intensely chlorite altered section of the clastic rock, together with minor amounts of disseminated pyrite, c) "prior to sulphide deposition", unreplaced portion of the hanging-wall sequence, consisting of fine-grained, impermeable shale and volcaniclastic rocks showing a conformable transition, appearing to represent the pre-replacement lithology prior to sulphide deposition, d) "following the sulphide deposition", fine-grained shale with chlorite-quartz-pyrite alteration and minor graphite remnants, transitioning to massive sulphide, which represents the hydrothermal replacement processes in the volcaniclastic rocks (e.g., the one in "c"), e) pyrite and chalcopyrite-rich massive sulphide displaying replacement texture as irregular patches with chlorite and white mica represent the relict sections of the host clastic rocks, f) chalcopyrite-rich banded texture, parallel primary bedding/foliation, g) cataclastic massive sulphide, including remobilized chalcopyrite, h) photomicrograph of a polished thin section displaying high abundances of covellite and chalcocite as a replacement of chalcopyrite in a MS zone with copper grades up to 20 wt%. Abbreviations: Ep=epidote, Chl=chlorite, WMic=white mica, Act=actinolite, Qtz=quartz, Fsp=plagioclase feldspar, Mus=muscovite, Gra=graphite, Py=pyrite, Cpy=chalcopyrite, Cov= covellite, Cc=chalcocite, FW= ootwall, HW=hanging-wall.

quartz-mica-graphite assemblages, well-developed foliation and fissility, mostly forming the uppermost levels of the main mineralization. They generally show conformable transition with the volcaniclastic rocks in the hanging wall (Figure 3c). The fine-grained, organic matter bearing phyllites are impermeable and acted as a barrier, effectively confining the mineralizing fluids for sulphide deposition (Figure 3 c,d). The mineralized zones are identified with disseminated, banded, pyritic clastic, semi-massive, and massive sulphide textures. Textural features such as disseminated sulphides, hydrothermally altered patches of host rock (Figure 3e), stratiform banding (Figure 3f) and clastic fragments incorporated within sulphide layers indicate that mineralization largely formed through subseafloor replacement processes within relatively permeable volcaniclastic and clastic units adjacent to rift-related structures. These conditions enhanced fluid-rock interaction at depth, promoted metal deposition, and contributed to the large size (e.g., Figure 2) and locally high grades of the Karaburun deposit (e.g., western zone of the ore body). Remobilization is present through the sulphide minerals due to subsequent metamorphism processes (Figure 3g). Secondary copper sulphides, such as bornite, covellite, and chalcocite, representing supergene enrichment, have partially to completely replaced chalcopyrite and sphalerite (Figure 3h).

MATERIALS AND METHODS

Fluid inclusions

Quartz-bearing mineralized samples were collected from the central and western sectors of the Karaburun deposit, preferentially targeting Cu-rich specimen. This strategy was adopted because the western domain is inferred to host higher Cu grades, potentially reflecting closer proximity to feeder zones (e.g., Slack et al., 2024; Çavdar et al., 2025b). Where stockwork or discrete feeder conduits are absent, these samples are considered the best available proxies for constraining ore-forming conditions; therefore, the resulting measurements and calculations are interpreted to approximate the physicochemical properties of the mineralizing hydrothermal fluids. Accordingly, sampling focused on representative mineralized domains, including massive sulphide with silicified relict patches (Figure 4a), intensely silicified central parts of the ore zones (Figure 4b), quartz-bearing hydrothermally altered intervals within semi-massive sulphide (Figure 4c), and well-developed bedding-parallel chalcopyrite-pyrite bands containing quartz (Figure 4d) suitable for fluid inclusion petrography and microthermometry.

Double-polished, 80-µm-thick sections were prepared at the General Directorate of Mineral Research and Exploration, Department of Mineral Analysis and Technology. Fluid inclusion petrography and microthermometry were conducted at the İstanbul Technical University fluid inclusions laboratory using a Linkam THMG-600 heating-freezing stage operating from -200 to +600 °C. Freezing and heating measurements were acquired following standard procedure (Roedder, 1984; Shepherd et al., 1985), with stated uncertainties of ±0.4 °C (freezing) and ±5.0 °C (heating). Inclusions were examined using a Leica DM2500P optical microscope; video records and photomicrographs were collected to document inclusion populations. Homogenization temperature (T_h), eutectic temperature (T_e), and final ice-melting temperature ($T_{m\text{-}ice}$) were measured and recorded (Figure 5). Bulk salinity values (wt% NaCl equiv.) were calculated using the equations of Bodnar (1993).

Isotope analyses

Oxygen isotope compositions of quartz ($\delta^{18}O$; n=10) were measured at the Stable Isotope Laboratory, University of Lausanne (Switzerland). Hand-picked quartz separates were prepared under a binocular microscope and submitted for analysis. Quartz powders were analysed on a Finnigan MAT 253 mass spectrometer coupled to an extraction line with a CO_2 laser system, using F_2 as reactant gas. Prior to fluorination, samples were dried at 180 °C for 24-48 hours, then evacuated under vacuum for ≥10 hours to minimize adsorbed water. After repeated pre-fluorination, quartz was reacted by CO_2-laser heating in 50 mbar of pure F_2. Excess F_2 was converted to Cl_2 using KCl at 150 °C and separated from O_2; the liberated O_2 was trapped on a molecular sieve and introduced to the mass spectrometer. Data were calibrated against the quartz standard LS-1 (17.83±0.026 ‰) and reported relative to Vienna Standard Mean Ocean Water (VSMOW).

Lead concentrations and isotope ratios (^{208}Pb, ^{207}Pb, ^{206}Pb, and ^{204}Pb) were determined for massive sulphide samples (n=4) by HR-ICP-MS at the laboratories of Turkish Energy, Nuclear and Mineral Research Agency; method performance criteria were evaluated as part of the analytical workflow. In this study, analytical-grade HBr, HCl, HF, and HNO_3 were used throughout, with ultrapure water (18.2 MΩ; Milli-Q) for dilutions and rinses. Lead was purified using Bio-Rad AG1-X8 anion-exchange resin. SRM981 (National Institute of Standards and Technology, USA) was employed for mass bias correction and results were additionally checked against the ERM-AE142 isotopic Pb standard. For digestion, 100-110 mg of each sample was weighed into 100 mL Teflon beakers and treated with 10 mL HNO_3 plus 1 mL HF. Complete dissolution was achieved at 230 °C for 1 hour under high pressure/temperature conditions. Digests were dried on a hotplate, then brought to 50 mL with 1%

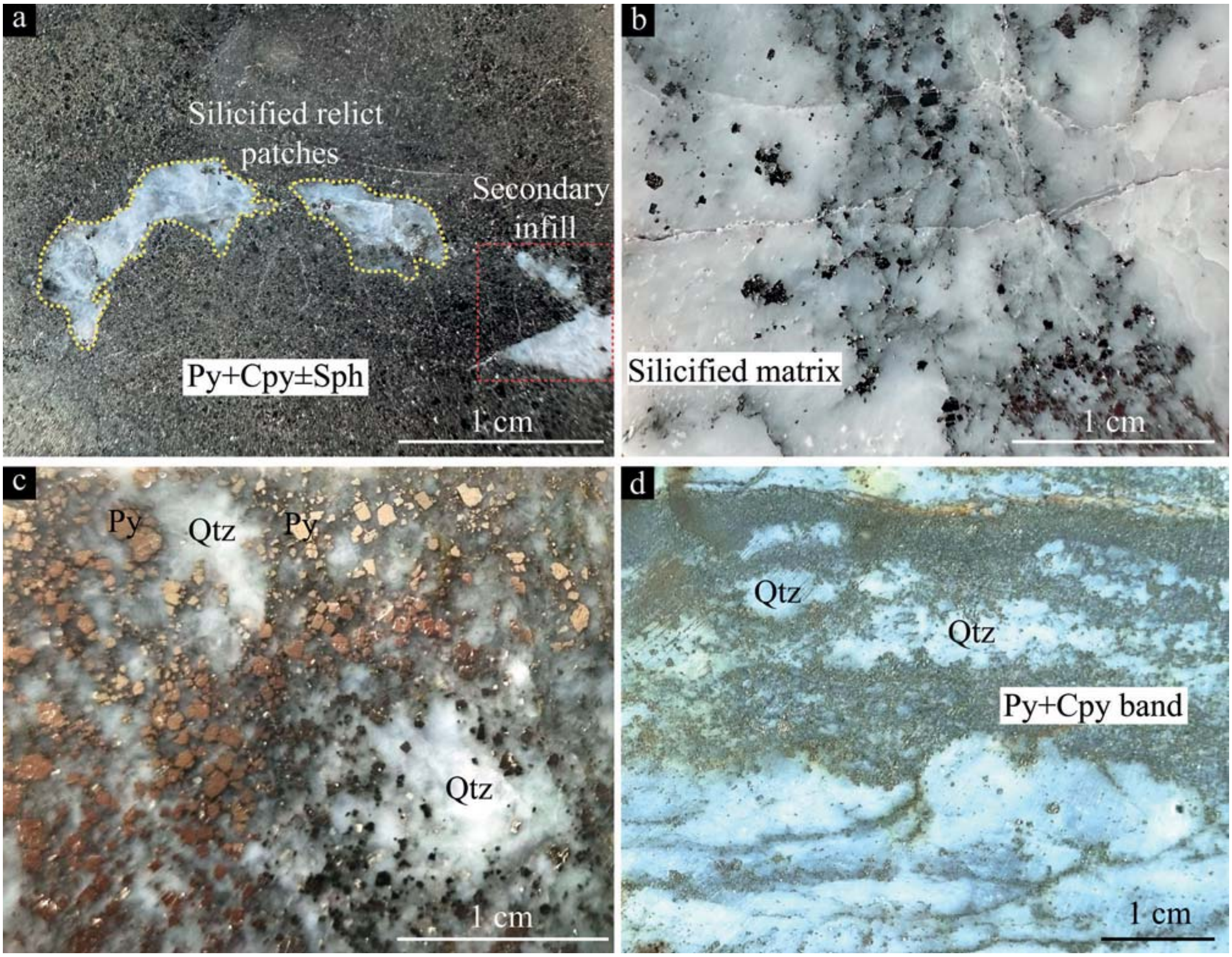

Figure 4. Selected examples from the mineralized zones for fluid inclusion studies. a) Massive sulphide zone containing silicified relict patches, b) sample from the central part of the mineralized zone with a highly silicified matrix, c) quartz-bearing hydrothermally altered sections within the semi-massive zone, d) well-developed chalcopyrite-pyrite band conformable with primary bedding, showing the quartz analysed for fluid inclusions. Abbreviations: Qtz=quartz, Py=pyrite, Cpy=chalcopyrite, Sph=sphalerite.

(v/v) HNO_3; aliquots were taken for concentration and isotope determinations. For isotope work, split aliquots were re-dried and re-dissolved in 10 mL of 0.5 M HBr before column loading. Columns were conditioned and washed sequentially with 4 mL of 6 M HCl, 5 mL of Milli-Q H_2O, and 10 mL of 0.5 M HBr; sample in 0.5 M HBr were then loaded. Under these conditions, most matrix cations (Al, Fe, Na, K, Ti, Mg, Ca, Mn, Sr, Ba, etc.) pass through the resin, whereas Pb is retained and subsequently eluted with 5 mL of concentrated HCl (10.8 M). Additional verification procedures, comparable to those outlined by Unruh et al. (2000) using soil reference materials (NIST 2709, 2710, and 2711) were also applied, further supporting the accuracy and reproducibility of the Pb isotope data for the Karaburun massive sulphides.

RESULTS

Fluid inclusion petrography and microthermometric data

Fluid inclusion (FI) work was completed on quartz from quartz-rich semi-massive sulphide, massive sulphide, and pyritic clastic samples because a feeder/stockwork level suitable for FI sampling has not been identified in the Karaburun deposit (Çavdar et al., 2025b). Sphalerite was also examined, but no FIs were observed; the fine-grained nature of the sphalerites limited FI detection. Consequently, FI measurements targeted quartz only. All measurements were conducted on two-phase (liquid + vapor) inclusions. Inclusions are mostly irregular; locally, inclusions aligned with quartz growth zones display more regular geometric shapes. Due to the small size and scarcity of the FIs, no grouping was applied. In total, 30 measurements were obtained from primary inclusions in quartz minerals (Table 1).

In primary inclusions, the liquid phase occupies approximately 84 vol.% and the vapor phase ~16 vol.% (range: 7-26%; Table 1). Inclusion areas range from 6.6 to 85.7 μm^2. Eutectic temperature (T_e; n=25) vary from -10.9 to -26.0 °C (mean: -20.8 °C). Homogenization temperatures (T_h; vapor disappearance) range from 178 to 301 °C (mean: 214±25 °C; Table 1; Figure 6a). Final ice-melting temperatures (T_m) range from -0.8 to -7.5 °C

Table 1. Microthermometric data of different quartz minerals from the Karaburun deposit. Abbreviations: Te=eutectic temperature (°C), Tm=final ice-melting temperature (°C), Th=homogenization temperature (°C), L.A.=liquid area (μm^2), V.A.=vapor area (μm^2), Salinity=wt% NaCl, V/L=vapor area/liquid area, P=primary inclusion, Max.=maximum, Min.=minimum, and STD=standard deviation.

	Te	Tm	Th	L. A.	V. A.	Salinity	V/L	Type
1	-23.9	-5.3	235	44.5	7.0	8.28	0.16	P
2	-18.6	-5.1	213	10.3	2.0	8.00	0.19	P
3	-15.3	-4.9	203	20.8	4.5	7.73	0.22	P
4	-21.2	-5.4	220	25.4	5.7	8.41	0.22	P
5	-26.0	-4.9	216	25.6	3.1	7.73	0.12	P
6	-24.9	-5.7	206	28.5	3.8	8.81	0.13	P
7	-22.2	-4.6	218	25.1	4.9	7.31	0.20	P
8	-22.6	-2.4	215	85.7	8.5	4.03	0.10	P
9	-17.2	-5.3	223	29.8	3.1	8.28	0.10	P
10	-23.6	-4.6	222	51.3	6.6	7.31	0.13	P
11	-22.2	-2.7	278	10.3	1.5	4.49	0.15	P
12	-22.2	-2.3	195	31.0	3.8	3.87	0.12	P
13	-13.3	-1.2	206	35.8	3.5	2.07	0.10	P
14	-	-0.8	186	39.1	4.9	1.40	0.13	P
15	-21.7	-1.0	193	30.0	3.5	1.74	0.12	P
16	-25.2	-5.2	301	30.7	3.5	8.14	0.11	P
17	-21.3	-4.8	227	39.6	8.0	7.59	0.20	P
18	-12.3	-4.7	215	11.1	2.3	7.45	0.21	P
19	-19.9	-4.9	200	20.3	5.2	7.73	0.26	P
20	-24.3	-7.3	200	10.5	2.0	10.86	0.19	P
21	-21.0	-4.7	205	11.5	2.7	7.45	0.23	P
22	-10.9	-5.6	178	10.8	2.5	8.68	0.23	P
23	-25.0	-2.2	215	-	-	3.71	-	P
24	-20.5	-4.4	185	-	-	7.02	-	P
25	-20.2	-1.8	206	-	-	3.06	-	P
26	-24.9	-2.2	230	32.3	2.3	3.71	0.07	P
27	-20.1	-7.5	235	-	-	11.10	-	P
28	-	-3.4	185	29.4	3.4	5.56	0.12	P
29	-	-3.5	215	6.6	1.3	5.71	0.20	P
30	-	-4.6	205	14.9	2.5	7.31	0.17	P
Max.	-10.9	-0.8	301	85.7	8.5	11.10	0.26	
Min.	-26.0	-7.5	178	6.6	1.3	1.40	0.07	
Mean	-20.8	-4.1	214	27.3	3.9	6.50	0.16	
Std.	4.0	1.7	25	16.5	1.9	2.50	0.05	

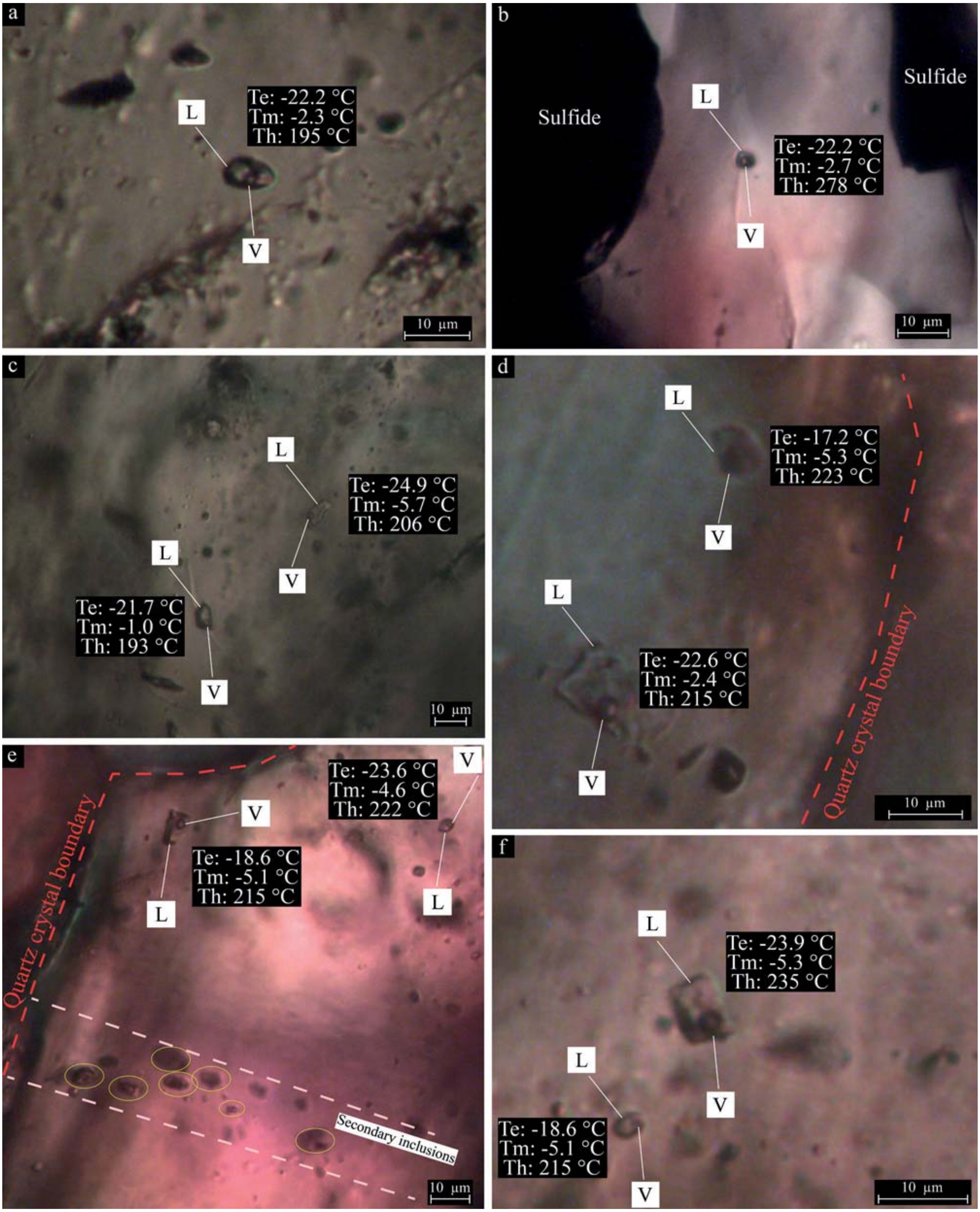

Figure 5. (a-f) Selected transmitted light photomicrographs and the data of fluid inclusions from mineralized sections. Abbreviations: V=vapor phase, L=liquid phase, T_h=homogenization temperature and T_e=eutectic temperature.

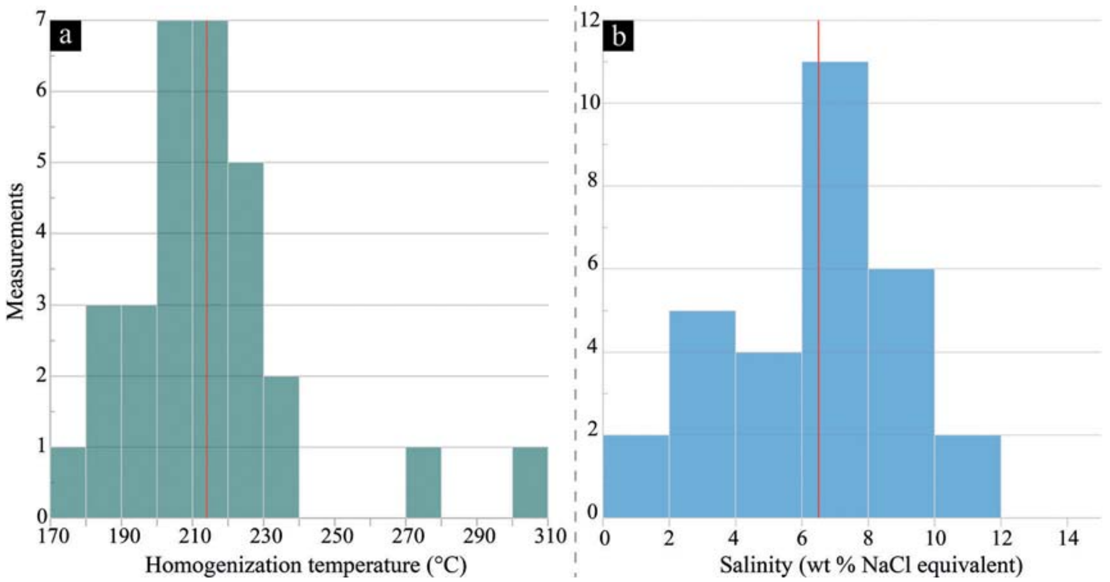

Figure 6. a) Distribution of homogenization temperatures measured in primary inclusions, b) salinity values calculated from T_m of fluid inclusions. Red lines indicate the exact mean values of the measurements.

(mean: -4.1±1.7 °C). Salinities calculated from T_m range from 1.4 to 11.1 wt% NaCl equiv. (mean: 6.5±2.5 wt%; Table 1; Figure 6b).

Pressure corrections were applied to convert measured T_h into trapping temperature, following established fluid-inclusion procedures (Potter, 1976; Roedder and Bodnar, 1980; Hurai, 2010; Lecumberri-Sanchez et al., 2012). In two-phase (liquid + vapor) FIs, homogenization is reached when the inclusion becomes a single phase (either liquid or vapor). Accordingly, the observed T_h represents homogenization at the pressure conditions relevant to the measurement rather than the original entrapment conditions. Where entrapment pressure is constrained or can be reasonably estimated, T_h requires pressure correction to recover the true trapping temperature (Roedder and Bodnar, 1980; Hurai, 2010). For the Karaburun deposit, a hydrostatic pressure equivalent to ~1600 m seawater depth was adopted for the correction, consistent with prior interpretations (Galley et al., 2007; Monecke et al., 2014; Tornos et al., 2015; Çavdar et al., 2025 a,b). Hydrostatic pressure was estimated using $P=\rho gh$ (density ρ; gravitational acceleration g; and water depth h); using an mean seawater density of $\rho \approx 1.025 \cdot 10^3$ kg m^{-3} and g=9.81 m s^{-2}, the pressure at 1600 m depth is approximately 161 bar. Including atmospheric pressure yields ~162 bar, and approximate correction of 160 bar was therefore applied. Pressure-corrected trapping temperatures were calculated using the HOKIEFLINCS_H_2O-NaCl software (Steele-MacInnis et al., 2012). The pressure-corrected dataset indicates a mean trapping temperature of 223±25 °C, with most values concentrated between ~200 and 250 °C. Compared with uncorrected T_h, applying the pressure correction increases estimated temperatures by ~10 °C.

Oxygen isotopes

Quartz samples from the mineralized zones of the Karaburun VMS deposit yield $\delta^{18}O_{(VSMOW)}$ values of 11.79 ‰ to 14.40 ‰ (mean: 12.92 ‰; standard deviation (SD): 0.85 ‰; Table 2). Hydrothermal fluid compositions ($\delta^{18}O_{(fluid)}$) were calculated from quartz $\delta^{18}O$ values using quartz-water fractionation relationships and standard calculation procedures (Clayton et al., 1972; Taylor, 1974; Arnold and Sheppard, 1981; Taylor, 1987; Sharp and Kirschner, 1994) (Table 2). The pressure-corrected FI temperature (223 °C) was used as the calculation temperature, and values were also computed at 200 and 250 °C, calculations were additionally reported at 300 °C (Hannington et al., 1995; Ohmoto, 1996; Goodfellow et al., 2003). Calculated $\delta^{18}O_{(fluid)}$ ranges (with means) are: 0.02 ‰ to 2.60 ‰ (mean: 1.13 ‰) at 200 °C; 2.77 ‰ to 5.36 ‰ (mean: 3.89 ‰) at 250 °C; and 4.84 ‰ to 7.44 ‰ (mean: 5.96 ‰) at 300 °C (Table 2). Oxygen isotope datasets and calculations of this type are routinely reported in ore deposit studies (e.g., Gökçe and Bozkaya, 2007; Akaryali et al., 2016; İmer et al., 2016; Kaya et al., 2023).

Lead isotopes

Common Pb isotope ratios were measured on whole-rock massive sulphide samples (e.g., Tessalina et al.,

Table 2. General information on the samples analysed for oxygen isotopes, along with the measured $\delta^{18}O_{(qtz)}$ and calculated $\delta^{18}O_{(fluid)}$ (VSMOW) values based on different temperature references. Equation proposed by Clayton et al. (1972): $1000\ln\alpha=(3.38\cdot10^6/T^2)-3.40$; $\alpha_{mineral\text{-}fluid}=\delta^{18}O_{mineral\text{-}fluid}$. Abbreviations: Qtz=quartz, SMS=semi-massive sulphide, MS=massive sulphide, DS=disseminated texture and BN=banded texture.

Sample	Drillhole ID	Depth (m)	Ore texture	$\delta^{18}O_{(qtz)}$	$\delta^{18}O_{(fluid)}$	$\delta^{18}O_{(fluid)}$	$\delta^{18}O_{(fluid)}$
				Analysed	Reference T(°C)=200	Reference T(°C)=250	Reference T(°C)=300
KIO-1	SKD-45	91.8	SMS-MS	12.39	0.62	3.37	5.44
KIO-2	SKD-45	106.5	DS	11.83	0.06	2.81	4.88
KIO-3	SKD-45	122.0	SMS	12.97	1.19	3.94	6.02
KIO-4	SKD-45	146.7	SMS-MS	12.73	0.95	3.71	5.78
KIO-5	SKD-45	152.5	MS	13.54	1.75	4.51	6.58
KIO-6	SKD-45	191.0	DS-BN	13.92	2.13	4.89	6.96
KIO-7	SKD-45	221.0	MS	14.40	2.60	5.36	7.44
KIO-8	SKD-48	99.6	DS-BN	12.09	0.32	3.07	5.14
KIO-9	SKD-48	102.6	DS	11.79	0.02	2.77	4.84
KIO-10	SKD-48	128.7	DS	13.49	1.70	4.46	6.53
			Minimum	11.79	0.02	2.77	4.84
			Maximum	14.40	2.60	5.36	7.44
			Mean	12.92	1.13	3.89	5.96

2016). In the Karaburun deposit, samples were collected from the 212.00-216.00 m interval of drill hole SKD154, where sulphides constitute approximately 50-60% of the rock volume. The lower part of the mineralized sampled interval is clastic-fragmental, containing coarse to very fine-grained pyrite and pyrite aggregates; upsection, the interval grades into a dense massive sulphide zone with a coherent texture and increased chalcopyrite, with silica-banded layers present in the upper part. Chalcopyrite is the dominant sulphide, and the assemblage includes pyrite and sphalerite with minor galena.

Lead isotope ratios determined from one-meter drill core intervals, together with the Cu-Pb-Zn concentrations, are reported in Table 3. Measured ratios fall within: $^{208}Pb/^{204}Pb$=37.4634-37.7507; $^{207}Pb/^{204}Pb$=15.4239-15.5032; and $^{206}Pb/^{204}Pb$=18.0790-18.4312. These measurements are reported alongside established applications of Pb isotopes in sulphide and VMS studies (Ohmoto, 1972; Sato and Sasaki, 1980; Sato et al., 1981; Huston, 1999; Shanks III, 2001; Franklin et al., 2005; Seal, 2006; Gill et al., 2019; Günay et al., 2022; Huston and Champion, 2023).

DISCUSSION

Characteristics of ore-forming hydrothermal fluids

The eutectic temperature (T_e) is determined by first freezing an individual fluid inclusion (FI) until complete solidification is achieved and then reheating until the first detectable liquid appears; this temperature marks the onset of eutectic melting and provides a first-order constraint on dissolved salt systematics. In Karaburun quartz-hosted FIs, T_e values (Table 1) span -26.0 °C to -10.9 °C (n= 25), clustering around mean of ~ -20.8±4 °C. Such T_e values are inconsistent with strongly CO_2^- or CH_4-rich systems and instead point to a dominantly aqueous saline fluid. Clathrate formation-solid hydrate phases associated with CO_2^- or CH_4-bearing inclusions-commonly occurs where these gases are abundant (Hou et al., 2008). Pure CO_2 has a eutectic at -56.6 °C, and CO_2 clathrate-melting temperatures ($T_{m(clt)}$) is typically expressed by final melting between approximately -1.5 to +9 °C (Shepherd et al., 1985). Methane-bearing systems generally show clathrate melting at >+10 °C ($T_{m(clt)}$>+10 °C). Where dissolved salts are significant, $T_{m(clt)}$ can be depressed below +10 °C and T_e may shift toward the H_2O-NaCl-CO_2 system (T_e≈-52 °C) (Shepherd et al., 1985). In the Karaburun dataset, no clathrate textures or melting were not observed during microthermometry, and T_e values are far above CO_2^- (or H_2O-NaCl-CO_2^-) dominated regime. Together, these observations support a dominantly H_2O-NaCl fluid system (Shepherd et al., 1985; Goldstein and Reynolds, 1994).

In general, the pressure-corrected homogenization (trapping) temperatures and salinities further constrain the ore-forming fluid. The Karaburun hydrothermal fluids show trapping temperatures averaging ~223±25 °C and salinities averaging ~6.5 wt% NaCl equivalent

Table 3. The $^{208}Pb/^{204}Pb$, $^{207}Pb/^{204}Pb$, and $^{206}Pb/^{204}Pb$ results of selected samples along with the geochemical concentrations of the main base metals (in ppm) for each corresponding sampling interval. See Figure 2 for the drillhole collar.

Drillhole	Sample	From	To	Cu	Zn	Pb	$^{208}Pb/^{204}Pb$	$^{207}Pb/^{204}Pb$	$^{206}Pb/^{204}Pb$
SKD154	J197	212.00	213.00	7599	2167	48	37.490	15.424	18.143
	J198	213.00	214.00	23015	2540	72	37.751	15.503	18.431
	J199	214.00	215.00	42095	5539	123	37.463	15.448	18.079
	J201	215.00	216.00	43831	6203	142	37.493	15.430	18.040

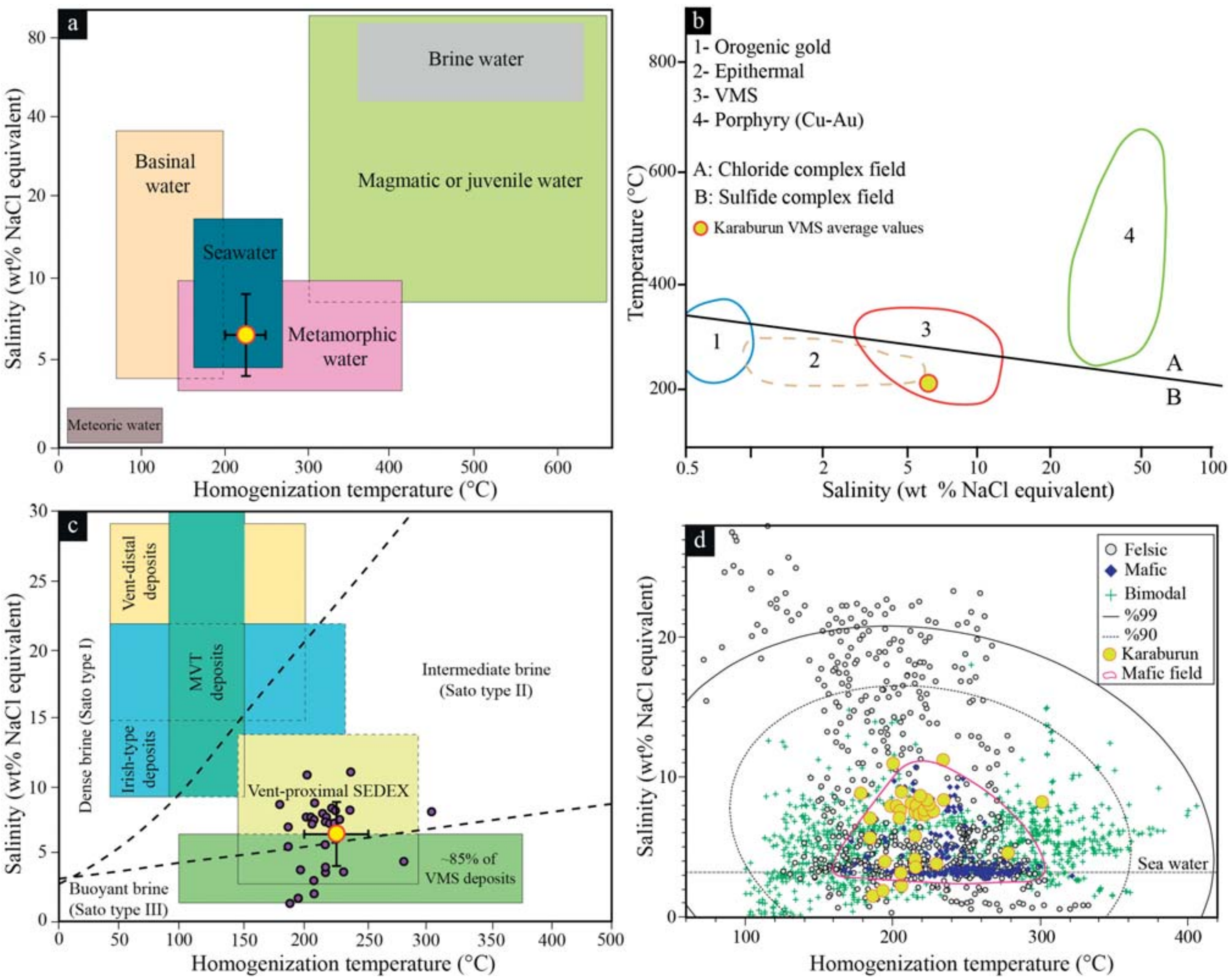

Figure 7. Homogenization temperature (°C) vs. salinity (wt% NaCl equiv.) plots of the Karaburun VMS deposit based on fluid inclusion data. a) Diagram showing the characteization of oreforming fluid source based on the mean salinity and temperature values of Karaburun (after Kesler, 2005); b) fields defined for different hydrothermal ore systems on the temperature-salinity diagram (after Misra, 2000; Wilkinson, 2001); c) temperature-salinity plot showing the distribution fields of dense, intermediate, and buoyant brines, along with the characteristic salinity-temperature ranges of oreforming fluids from various hydrothermal deposit types, including MVT, Irishtype, ventdistal and ventproximal SEDEX, and VMS systems (adapted from Fakhri-Doodoui and Alipour-Asll, 2024). Data sources: Gardner and Hutcheon (1985), Ansdell et al. (1989), Cooke et al. (2000), Sangster (2002), Leach et al. (2005), Wilkinson et al. (2009), Wilkinson (2010), Bodnar et al. (2014); d) summary of published homogenization temperaturesalinity pairs from VMS deposits (from Bodnar et al., 2014), and distribution of fluid inclusion measurements in temperature vs salinity plot.

(Table 1; Figure 7a). These conditions are broadly consistent with ore forming fluids in VMS settings that are largely derived from seawater and variably modified during subseafloor circulation (Wilkinson, 2001; Vanko et al., 2004; Bodnar et al., 2014). In the context of VMS deposit formation and the proposed genetic framework for the Karaburun deposit, a seawater-dominated fluid source is therefore plausible. Nevertheless, the mean salinity of ~6.5 wt% NaCl equivalent is modestly elevated relative typical seawater-derived VMS fluids, which commonly cluster near ~3.2 wt% NaCl equivalent (Bischoff and Rosenbauer, 1985), even though higher salinities are known in some VMS subtypes (e.g., pelitic-mafic VMS systems such as Windy Craggy, reaching ~17 wt% NaCl equivalent; Peter and Scott, 1999) (Figure 7 b,c). While Archean VMS inclusions can record salinities above modern seawater that have been linked to secular seawater chemistry changes (de Ronde et al., 1997), such reasoning is not applicable to Mesozoic mineralization and cannot be invoked to explain the Karaburun values. Consequently, the Karaburun fluids are best described as seawater-derived by slightly (and systematically) more saline than typical seawater-like VMS fluids (Figure 7c). Elevated salinity in subseafloor hydrothermal system may develop through several mechanisms, including (i) water-rock interaction and leaching during deep circulation, (ii) phase separation/boiling, (iii) dissolution of evaporites or other saline sedimentary components, and/or (iv) addition of magmatic volatiles and/or fluids (Wilkinson, 2001; Pirajno, 2009; Bodnar et al., 2014; Kiss, 2015). For Karaburun, evaporite-related explanations appear unlikely. There is no indication of sulphate-bearing fluids (e.g., from sulphur-isotope constrains; Çavdar et al., 2025b), and barite, a common sulphate phase in many VMS settings (e.g., Ohmoto, 1996; Barrie and Hannington, 1999; Solomon et al., 2004; Badrzadeh et al., 2011), is also absent. Moreover, no evaporites/gypsum minerals are reported either syn- or post-mineralization, making evaporite dissolution an improbable driver of salinity (e.g., Peter and Scott, 1999).

Boiling/phase separation can generate brine and increase salinity in some vent complexes (Butterfield et al., 1990), where temperatures are high and/or confining pressure is low (Monecke et al., 2014; Tornos et al., 2015). Thermodynamic constraints indicate that at ~1500 m water depth, pure seawater boils near 342 °C, and a ~6 wt% NaCl equiv. solution near 344 °C (Driesner and Heinrich, 2007). Such temperatures exceed those recorded in the Karaburun FIs, where the maximum measured temperature T_h is ~301 °C (Table 1). In addition, the dominance of two-phase (L+V) inclusions with comparatively consistent vapor fractions argues against widespread boiling/phase separation at entrapment conditions. Using temperature-pressure-depth relations for seawater (3.2 wt% NaCl equiv.; Bischoff and Rosenbauer, 1985) and a representative high-salinity fluid (10 wt% NaCl equiv.; after Roedder and Bodnar, 1980), the Karaburun maximum temperature and inclusion phase proportions imply that a minimum water depth of ~850 m (hydrostatic pressure ~85 bar) would be sufficient to suppress boiling-similar to the interpretations from the pelitic-mafic Nudeh VMS system in Iran (Maghfouri et al., 2018). For conservative pressure correction of T_h to trapping temperature, a higher confining pressure of ~160 bar was adopted (Monecke et al. 2014), consistent with average depths suggested for back-arc rift environments in intra-oceanic arc settings. Overall, the lack of boiling and the absence phase separation indicators imply that these processes did not control the observed salinity in the Karaburun system.

Given the limited support for evaporite dissolution or boiling, the most plausible explanation for the modest salinity enrichment is seawater modification during deep circulation, potentially enhanced by heat and/or minor fluid input from a deeper intrusion. In many VMS districts, deeply emplaced intrusions are considered important heat sources that can influence fluid pathways, reaction progress, and ultimately fluid composition (Goodfellow and McCutcheon, 2003; Gemmell et al., 2004; Hou et al., 2008; Huston et al., 2011). At Karaburun, no intrusion has been intersected even in the deepest drill hole (~862.60 m), which penetrates serpentinite-dominated ophiolitic units and eclogites. Nevertheless, in the absence of stronger alternative mechanisms of the elevated salinity, a limited magmatic contribution remains a viable (but currently unconfirmed) hypnosis (Çavdar et al., 2025 a,b). Because mineralization developed near oceanic rifting and relatively distal to the volcanic arc, rift-related magmatic bodies could be involved; however, this remains speculative and requires deeper drilling. Any such intrusions would be expected to be geochemically and geochronologically compatible with the Karaburun VMS system and to leave additional geochemical fingerprints.

Isotopic constraints provide mixed support for magmatic involvement. Magmatic sulphur is typically characterized by $\delta^{34}S \approx 0 \pm 2$ ‰ (Hoefs, 2009) and can produce negative sulphides values in many hydrothermal systems (Rye, 1993; Huston et al., 2011). The absence of clear magmatic sulphur signal at the Karaburun deposit (Çavdar et al., 2025b) weakens a strong magmatic-fluid interpretation. Conversely, magmatic fluids commonly have elevated $\delta^{18}O$ values inherited from source magmatic rocks, typically ranging from 5.5 to 13 ‰ (Taylor, 1974; Arnold and Sheppard, 1981). The $\delta^{18}O$ measured in Karaburun quartz (11.79 to 14.40 ‰; Table 2) overlap the upper portion of this of magmatic-rock range (Hoefs, 1984), suggesting that the seawater-dominated fluids may have acquired a minor magmatic or high-$\delta^{18}O$ signature, either through limited magmatic fluid input and/or high-temperature exchange with igneous rocks

More broadly, Karaburun FI characteristics-absence of detectable CO_2, moderate salinity, and dominance of two-phase (L+V) inclusions-fall within the envelope typical for VMS deposits (Wilkinson, 2001; Vanko et al., 2004; Bodnar et al., 2014) (Figure 7 b,d). The lack of coexisting vapor-rich and halite-bearing inclusions, together with the predominance of the liquid phase (approximately L: 85%, V: 15%), indicates trapping in a near- to sub-seafloor environment. This further implies that the sedimentary cover above mineralization was not thick and that confining pressure was dominated by the overlying seawater column, consistent with the genetic model proposed for the Karaburun deposit (Çavdar et al., 2025 a,b).

Oxygen isotope constraints on fluid sources and conditions

Oxygen isotopes are a key tracer of hydrothermal processes because they constrain (1) fluid origin (e.g., seawater, meteoric, magmatic), (2) the nature aquifers supplying the system, (3) mixing relationship among distinct reservoirs, and (4) the extent and conditions of rock-fluid exchange (Taylor, 1974; Sheppard, 1981; Huston et al., 2023). Modern seawater is characterized by $\delta D \approx 0.20$ ‰ and $\delta^{18}O \approx 0.04$ ‰ (Attendorn and Bowen, 1997), and multiple studies indicate that seawater $\delta^{18}O$ has remained broadly stable since at least the Early Paleozoic (Sheppard, 1986; Knauth and Roberts, 1991). This long-term stability makes seawater a robust baseline for interpreting hydrothermal $\delta^{18}O$ signatures in Mesozoic VMS systems. In this study, the $\delta^{18}O$ values of hydrothermal fluids were calculated from quartz $\delta^{18}O$ (Table 2) using the quartz-water fractionation relationship of Clayton et al. (1972). Using representative temperatures of 200, 250, and 300 °C, the calculated $\delta^{18}O_{(fluid)}$ values span 0.02 ‰ to 7.44 ‰ (Table 2). When the mean value at 200 °C (1.13 ‰) is treated as a conservative lower bound and the mean at 300 °C (5.96 ‰) as the upper bound, the Karaburun hydrothermal fluids are best interpreted as dominantly seawater-derived with a subordinate magmatic contribution (Figure 8). This inference is consistent with the FI-based evidence for seawater-like fluids that were subsequently modified, as implied by the modest salinity enrichment.

Regional comparisons further support seawater dominance with possible magmatic influence. For VMS deposits in Türkiye, quartz $\delta^{18}O$ values of ~7.5 ‰ and 12.5 ‰ correspond to estimated $\delta^{18}O_{(fluid)}$ values of -0.6 ‰ to +2.9 ‰, interpreted as seawater-derived fluid and/or seawater-magmatic mixtures (Çiftçi, 2019) (Figure 8). For bimodal-mafic VMS deposits that are temporally and

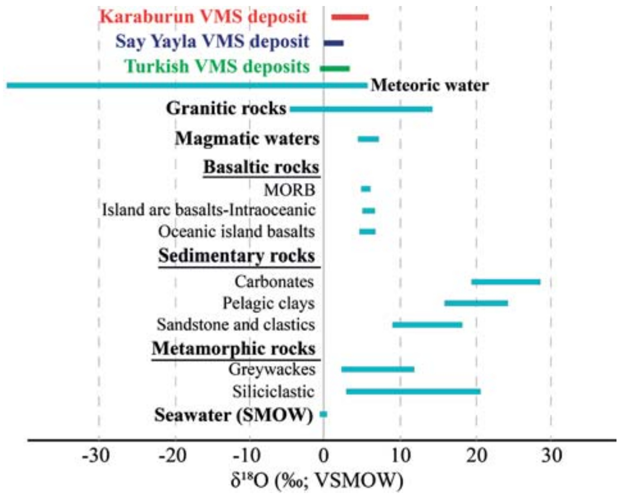

Figure 8. Comparison of oxygen isotope results with $\delta^{18}O$ ranges of various geological reservoirs. Data for the Say Yayla VMS deposit are from Günay et al. (2022), for other Turkish VMS deposits from Çiftçi (2019), and natural reference values are compiled from Grossman (1998), Hoefs (2021), and Rollinson and Pease (2021). The lower and upper limits of $\delta^{18}O$ values for the Karaburun VMS deposit were determined from $\delta^{18}O_{(fluid)}$ data calculated using the relevant isotopic fractionation equations.

spatially closely related to the Karaburun system, reported $\delta^{18}O_{(fluid)}$ ranges of ~0 ‰ to +2.4 ‰ similarly indicate a predominantly seawater reservoir with a potential magmatic contribution (Günay et al., 2022) (Figure 8).

To further evaluate formation temperatures under isotopic equilibrium, fluid-quartz equilibrium temperatures were calculated assuming $\delta^{18}O_{(VSMOW)}$ values of 0 ‰, 3 ‰, and 6 ‰ for hydrothermal fluid (Table 4). Under $\delta^{18}O_{(fluid)}=0$ ‰, calculated temperatures cluster at ~160-200 °C, whereas $\delta^{18}O_{(fluid)}=3$ ‰ yields ~205 to 253 °C (mean=231 °C), closely matching FI constraints and the intermediate-temperature regime typically inferred for VMS hydrothermal circulation. For $\delta^{18}O_{(fluid)}=6$ ‰, temperatures rise to ~262 to 333 °C (mean=301 °C), consistent with Cu-rich VMS conditions and the highest FI temperature observations. Collectively, these relationships suggest that the most plausible $\delta^{18}O$ composition of the Karaburun ore fluids lies between ~3 ‰ and 6 ‰, implying seawater that was isotopically shifted through interaction with rocks and/or limited magmatic addition. Given the near-constant seawater baseline of 0.00 ‰ through the Early Paleozoic (Sheppard, 1986; Knauth and Roberts, 1991), the elevated $\delta^{18}O_{(fluid)}$ range is consistent with seawater modification and align with the FI-derived salinity pattern.

Source of lead in massive sulphides

Lead production is recovered from several deposit

Table 4. General information on the samples analysed for oxygen isotopes, along with the measured $\delta^{18}O_{(qtz)}$ values and the corresponding calculated temperatures (T, °C) based on reference $\delta^{18}O_{(fluid)}$ values of 0 ‰, 3 ‰, and 6 ‰. The table also presents the maximum, minimum, and mean temperature values derived from the calculations based on equation proposed by Clayton et al., 1972: $1000\ln\alpha=(3.38\cdot10^6/T^2)-3.40$; $\alpha_{mineral-fluid=}\ \delta^{18}O_{mineral-fluid}$. Abbreviations: Qtz=quartz, SMS=semi-massive sulphide zone, MS=massive sulphide zone, DS=disseminated texture/level, BN=banded texture/level.

Sample	Drillhole ID	Depth (m)	Ore texture	$\delta^{18}O_{(qtz)}$	T (°C)$_{(qtz)}$	T (°C)$_{(qtz)}$	T (°C)$_{(qtz)}$
				Analysed	Reference	Reference	Reference
					$\delta^{18}O_{(fluid)}$=0 ‰	$\delta^{18}O_{(fluid)}$=3 ‰	$\delta^{18}O_{(fluid)}$=6 ‰
KIO-1	SKD-45	91,8	SMS-MS	12.39	190	241	314
KIO-2	SKD-45	106,5	DS	11.83	198	253	332
KIO-3	SKD-45	122	SMS	12.97	181	230	298
KIO-4	SKD-45	146,7	SMS-MS	12.73	185	234	305
KIO-5	SKD-45	152,5	MS	13.54	174	219	283
KIO-6	SKD-45	191	DS-BN	13.92	169	213	273
KIO-7	SKD-45	221	MS	14.40	163	205	262
KIO-8	SKD-48	99,6	DS-BN	12.09	194	247	324
KIO-9	SKD-48	102,6	DS	11.79	199	253	333
KIO-10	SKD-48	128,7	DS	13.49	174	220	284
			Minimum	11.79	163	205	262
			Maximum	14.40	199	253	333
			Mean	12.92	182	231	301

classes; notably shale-hosted Zn-Pb-Ag, Mississippi Valley-type Zn-Pb (including Irish-type), and VMS systems (Huston and Champion, 2023; Huston et al., 2023). The origin of Pb in such deposits is debated and may involve mantle and/or crustal reservoirs, direct magmatic-hydrothermal input, and/or leaching from host rocks (Huston et al., 2023). A useful first-order discriminator is that mantle-derived Pb is generally less radiogenic and more isotopically homogeneous than crustal Pb, which tends to be more radiogenic and variable due to diverse U-Th-Pb evolution histories.

The Karaburun VMS display a narrow, highly homogeneous, and comparatively less radiogenic Pb isotope range, most consistent with a mantle-dominated source. Available geochemical constrains indicate that much of the Pb was derived from depleted MORB mantle or a back-arc basin (BAB)-like reservoir (Figure 9), in agreement with the geological and geochemical character of the Karaburun basaltic host rocks and mineralization (Çavdar et al., 2025b).

To place these data in a broader tectonic framework, the plumbotectonic model uses Pb isotope ratios (^{206}Pb, ^{207}Pb, ^{208}Pb relative to ^{204}Pb) to infer metal sources and the tectono-crustal environment of ore formation (Tornos and Chiaradia, 2004; Basori et al., 2017; Deng et al., 2020). The model formalized by Zartman and Doe (1981) depicts evolutionary trends for major reservoirs (mantle, upper crust, lower crust, orogenic domains) and has been widely applied in metallogenic problems (Tessalina et al., 2016; Mao et al., 2018; Yu et al., 2020; Kahya and Kuşcu, 2022). Because Pb isotope ores track long-term U-Th decay in source regions, comparisons to these reservoir fields can provide robust constraints on the dominant Pb source.

In the Karaburun case, the massive sulphide Pb isotopic ratios plot within the mantle-derived source fields when evaluated against mantle, upper crust, lower crust, orogenic domains, and pelagic sediment reservoirs (Figures 10 and 11). In addition, Figure 12 compares Karaburun and other Pb mineralizations to the classical Pb-evolution curves of Cumming-Richards (Cumming and Richards, 1975) and Stacey-Kramers (Stacey and Kramers, 1975), which have been used to contextualize hydrothermal deposit ages and source evolution. Deposits spanning Archean (e.g., Manitouwadge and Noranda, Canada), Early Paleozoic (Outokumpu, Finland; Flin Flon, Canada), and Paleozoic-

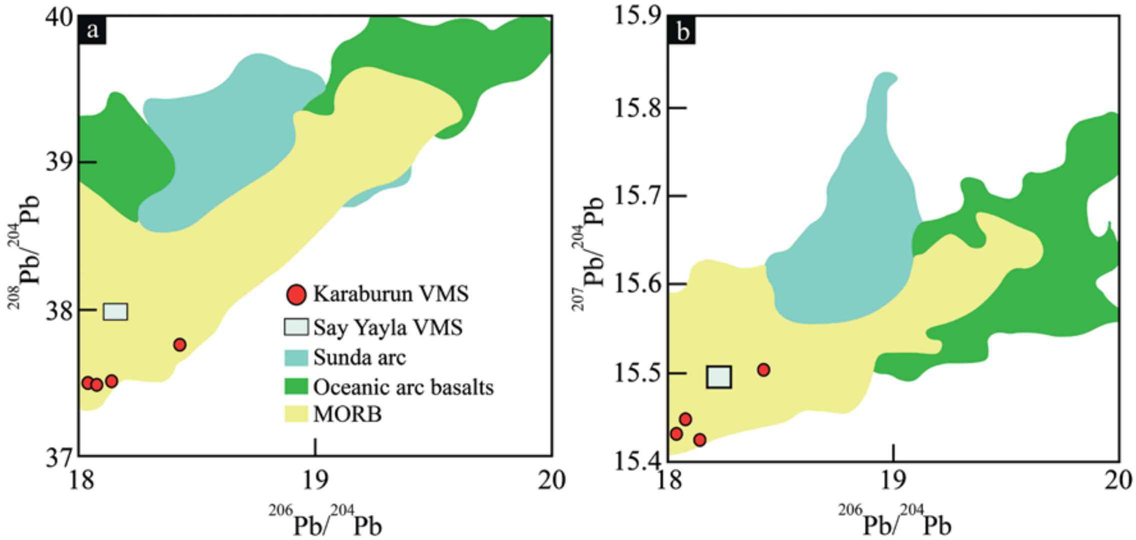

Figure 9. Diagrams of lead isotopes. a) $^{208}Pb/^{204}Pb$ vs. $^{206}Pb/^{204}Pb$, and b) $^{207}Pb/^{204}Pb$ vs. $^{206}Pb/^{204}Pb$. Data are from Chakrabarti et al. (2011), Çiftçi and Lermi (2014) and Günay et al. (2022).

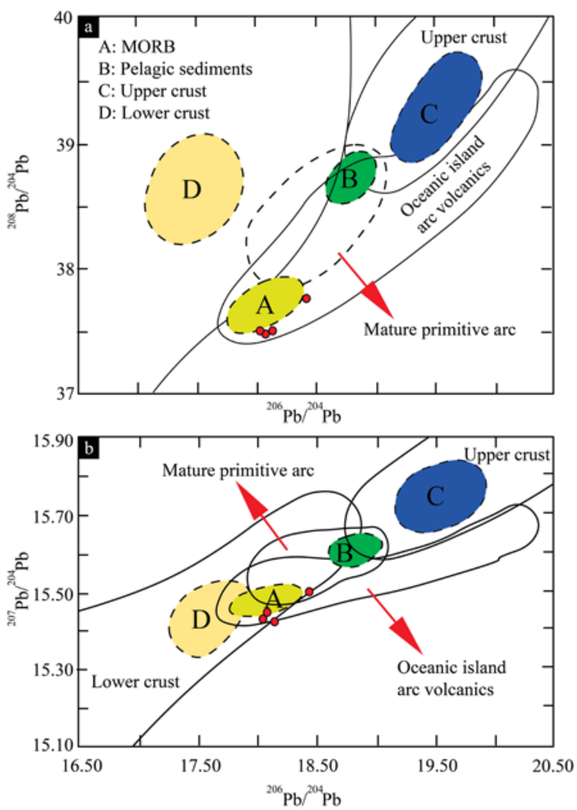

Figure 10. Summary diagrams of lead isotope ratios used to define modern fields for the mantle, upper crust, lower crust, and orogenic domains. a) $^{208}Pb/^{204}Pb$ vs $^{206}Pb/^{204}Pb$ diagram, b) $^{207}Pb/^{204}Pb$ vs. $^{206}Pb/^{204}Pb$ diagram. Solid lines encompass 80% of all data points for each field, while dashed lines outline the probable mean values (A=mantle; B=orogeny; C=upper crust; D=lower crust). Additional geological environments are also indicated. Diagrams are modified from Zartman and Doe (1981).

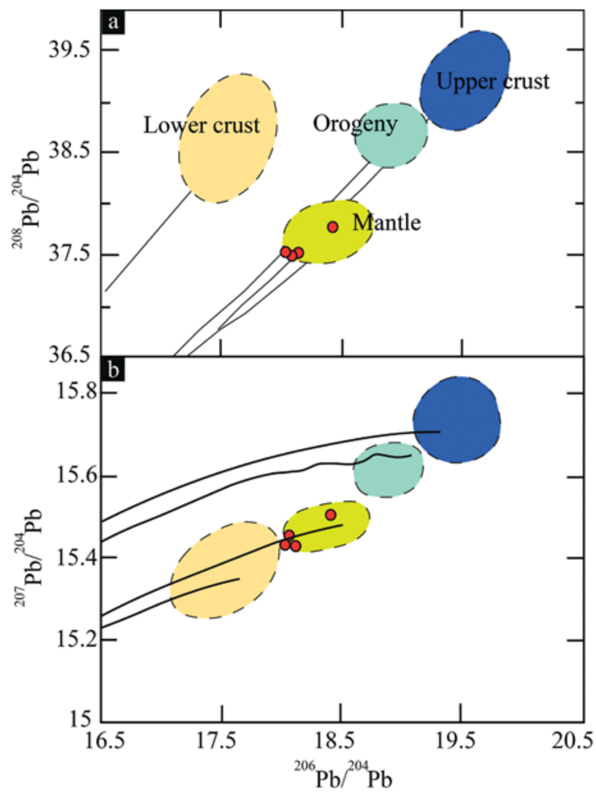

Figure 11. Fields showing the temporal evolution curves of lead isotopes for selected sources, along with their possible mean compositions (Zartman and Doe, 1981; Zartman and Haines, 1988). a) $^{208}Pb/^{204}Pb$ vs $^{206}Pb/^{204}Pb$ diagram; b) $^{207}Pb/^{204}Pb$ vs $^{206}Pb/^{204}Pb$ diagram.

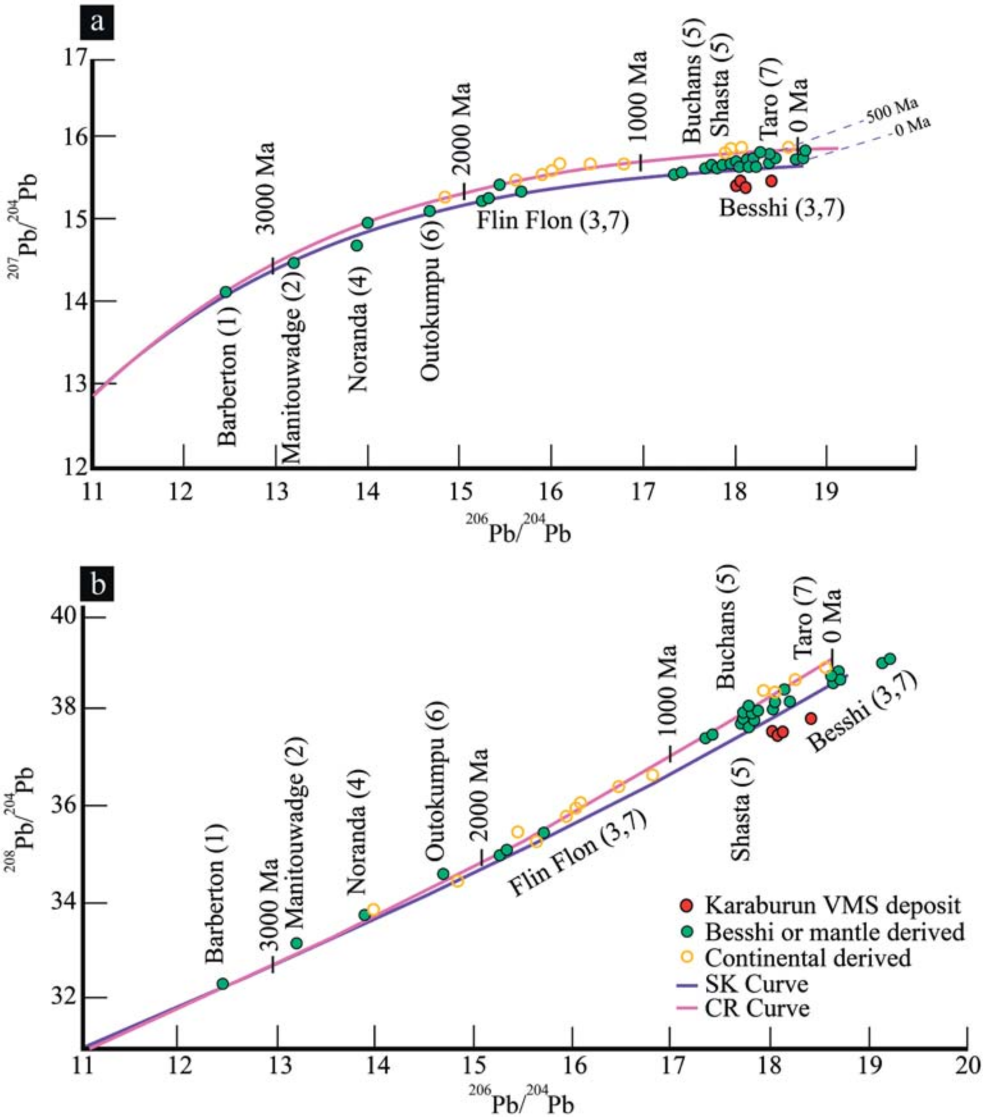

Figure 12. a) $^{207}Pb/^{204}Pb$ vs $^{206}Pb/^{204}Pb$ and b) $^{208}Pb/^{204}Pb$ vs $^{206}Pb/^{204}Pb$ diagrams showing the orelead evolution curves (Cumming and Richards, 1975; Stacey and Kramers, 1975) and the lead compositions of two types of stratiform deposits (continental and mantle-derived). Data sets are from Sato and Sasaki (1980).

Early Mesozoic (Shasta, USA; Buchans, Canada) can be evaluated in this framework as likely mantle-influenced systems (Sato and Sasaki, 1980). Notably, mafic-pelitic and mantle-derived Phanerozoic deposits show broadly similar Pb isotope fields (Figure 12a), with data lying along the lower portion of both curves, implying comparable time-integrated evolution and/or a shared mantle contribution. In the $^{208}Pb/^{204}Pb$-$^{206}Pb/^{204}Pb$ diagram (Figure 12b), Besshi/pelitic-mafic-type VMS and other mantle-derived Phanerozoic deposits likewise occupy the lower curves regions. This distribution has been interpreted to reflect a low Th/U ratio in the source than that implied by the reference growth curve (Sato and Sasaki, 1980; Kahya and Kuşçu, 2022). Sato and Sasaki (1980) further suggested that such Th/U effects may become especially evident in later Earth history, and the Karaburun dataset shows a slight tendency toward the Stacey-Kramers trajectory relative to Cumming-Richards (Figure 12).

Finally, the Karaburun VMS mineralization age (163.6±7.1 Ma; Late Jurassic, Early Oxfordian) (Çavdar et al., 2025b) is consistent with the position of the Pb isotope data along the growth curves and supports a broadly Mesozoic isotopic evolution. The Pb isotope systematics therefore indicate a mantle- or MORB-derived metal budget and possibly a mantle-related contribution to hydrothermal circulation, consistent with the proposed geodynamic setting of submarine mafic volcanism-related hydrothermal systems (Çavdar et al., 2025b). In turn, therefore, the combined Mesozoic affinity and mantle/MORB isotopic signature support interpretation of Karaburun formation in a Jurassic arc-back-arc framework, comparable to other VMS systems in the Central Pontides and analogous deposits reported regionally (Günay et al., 2022; Kahya and Kuşcu, 2022; Günay, 2023; Çavdar et al., 2025b).

CONCLUSIONS

Fluid-inclusion microthermometry and O-Pb isotope geochemistry reported here provide the first direct constraints on ore-fluid properties and metal sources for the giant Jurassic Karaburun pelitic-mafic VMS deposit of the Çangaldağ Metamorphic Complex (Central Pontides, Türkiye). Primary two-phase inclusions in ore-stage quartz yield T_e of -26 to -11 °C, show no clathrate behaviour, and therefore define a dominantly H_2O-NaCl fluid. Homogenization temperatures of 178-301 °C, corrected for ~160 bar hydrostatic pressure, indicate trapping at 223±25 °C, whereas ice-melting temperatures correspond to 1.4-11.1 wt% NaCl equiv. (mean 6.5 wt%). The combination of moderate, systematically elevated salinity and the lack of boiling/phase-separation textures favour seawater-derived fluids that were modified during deep subseafloor circulation, potentially aided by a minor magmatic component. Quartz $\delta^{18}O$ values of 11.8-14.4‰ (VSMOW) require isotopically shifted hydrothermal fluids; equilibrium calculations at FI-constrained temperatures imply $\delta^{18}O_{(fluid)}$ of ~3-6‰, consistent with substantial water-rock exchange and/or limited magmatic input. The massive sulphides display a tightly clustered range of Pb isotope compositions ($^{208}Pb/^{204}Pb$: 37.4634-37.7507; $^{207}Pb/^{204}Pb$: 15.4239-15.5032; $^{206}Pb/^{204}Pb$: 18.0790-18.4312) characterized by comparatively low radiogenic signatures. The restricted isotopic variability is consistent with a predominantly mantle-derived Pb source, supporting the tectono-magmatic framework proposed for the Karaburun VMS system. When considered together, the geological observations and the geochemical, geochronological, isotopic (S-O-Pb), and fluid-inclusion constrains indicate that the Karaburun deposit-expressed as pelitic-mafic and/or replacement-style mineralization-developed within a Jurassic ensimatic arc-related back-arc basin evolving under back-arc-rifting conditions. The ore-forming hydrothermal fluids were derived chiefly from seawater, but their chemistry was modestly overprinted by contributions from magmatic fluids and/or volatiles, implying limited yet discernible magmatic involvement during mineralization.

ACKNOWLEDGEMENTS

This research was carried out by the General Directorate of Mineral Research and Exploration (MTA, Ankara/Türkiye) as a part of the Central and Western Black Sea Metallic Mineral Exploration Project (2015/20263213041). Grateful thanks also to Ebru Coşkun Kavukçu (Department of Mineral Analysis and Technology, MTA) for her assistance during fluid inclusion petrography. Lead isotope analyses were carried out at the Turkish Energy, Nuclear and Mineral Research Agency (TENMAK) within the framework of project “A4.H1.F24”, which aims to collaborate with national institutions, enhance knowledge and experience sharing on lead isotope analysis, and develop new analytical methodologies, all of which are gratefully acknowledged for their valuable support and cooperation. We sincerely thank editorinchief Paolo Ballirano for providing detailed comments and suggestions on an early draft of the manuscript. We are also thankful to two anonymous reviewers for their insightful feedback and thorough reviews, which greatly improved the quality of the paper. Appreciation is extended to section editor of “Ore deposits and Environment” Silvano Mignardi for handling the review of an earlier version of the manuscript and for editorial guidance.

REFERENCES

Akaryali E., 2016. Geochemical, fluid inclusion and isotopic (O, H and S) constraints on the origin of Pb-Zn±Au vein-type mineralizations in the Eastern Pontides Orogenic Belt (NE Turkey). Ore Geology Reviews 74, 1-14.

Akbulut M., Oyman T., Çiçek M., Selby D., Özgenç İ., Tokçaer M., 2016. Petrography, mineral chemistry, fluid inclusion microthermometry and Re-Os geochronology of the Küre volcanogenic massive sulfide deposit (Central Pontides, Northern Turkey). Ore Geology Reviews 76, 1-18.

Alparslan G. and Dilek Y., 2018. Seafloor spreading structure, geochronology, and tectonic evolution of the Küre ophiolite, Turkey: A Jurassic continental backarc basin oceanic lithosphere in southern Eurasia. Lithosphere 10, 14-34.

Altun Y., Yılmaz H., Şiner İ., Yazar F., 2015. The Secrets of Massive Sulfide Deposits on Mid-Ocean Ridges and Küre-Mağaradoruk Copper Deposit. Bulletin of the Mineral Research and Exploration 150, 51-65.

Ansdell K.M., Nesbitt B.E., Longstaffe F.J., 1989. A fluid inclusion and stable-isotope study of the Tom Ba-Pb-Zn deposit, Yukon Territory, Canada. Economic Geology and the Bulletin of the Society of Economic Geologists 84, 841-856.

Arnold M. and Sheppard S.M.F., 1981. East Pacific Rise at latitude 21°N: isotopic composition and origin of the hydrothermal sulphur. Earth and Planetary Science Letters 56, 148-156.

Attendorn H.G. and Bowen R.N.C., 1997. Extraterrestrial matter. Radioactive and Stable Isotope Geology, 443-451.

Aygül M., Okay A.İ., Oberhänsli R., Sudo M., 2016. Pre-collisional accretionary growth of the southern Laurasian active margin, Central Pontides, Turkey. Tectonophysics 671, 218-234.

Badrzadeh Z., Barrett T.J., Peter J.M., Gimeno D., Sabzehei M., Aghazadeh M., 2011. Geology, mineralogy, and sulfur isotope geochemistry of the Sargaz Cu-Zn volcanogenic massive sulfide deposit, Sanandaj-Sirjan Zone, Iran. Mineralium Deposita 46, 905-923.

Baran C., Yeşilova Ç., Günay K., 2021. Geologic and geochemical properties of the mafic-clastic type Sarıseki volcanogenic massive sulfide deposit, Central Pontides, Turkey. Neues Jahrbuch Für Mineralogie - Abhandlungen 197, 165-184.

Barrie C.T. and Hannington M.D., 1999. Introduction: classification of VMS deposits based on host rock composition. Reviews in Economic Geology 8, 2-10.

Barrie C.T., Cathles L.M., Erendi A., Schwaiger H., Murray C., 1997. Heat and Fluid Flow in Volcanic-Associated Massive Sulfide-Forming Hydrothermal Systems. In C. T. Barrie and M. D. Hannington (Eds.), Volcanic Associated Massive Sulfide Deposits: Processes and Examples in Modern and Ancient Settings. Reviews in Economic Geology, 201-219.

Basori M.B.I., Zaw K., Meffre S., Large R.R., Wan Hassan W.F., 2017. Pb-isotope compositions of the Tasik Chini volcanic-hosted massive sulfide deposit, Central Belt of Peninsular Malaysia: Implication for source region and tectonic setting. Island Arc 26(2), e12177.

Bischoff J.L. and Rosenbauer R.J., 1985. An empirical equation of state for hydrothermal seawater (3.2 percent NaCl). American Journal of Science 285, 725-763.

Bodnar R.J., 1993. Revised equation and table for determining the freezing point depression of H_2O-Nacl solutions. Geochimica et Cosmochimica Acta 57, 683-684.

Bodnar R.J., Lecumberri-Sanchez, P., Moncada, D., Steele-MacInnis M., 2014. Fluid Inclusions in Hydrothermal Ore Deposits. In H. D. Holland and K. K. Turekian (Eds.), Treatise on Geochemistry. Elsevier, 119-142.

Butterfield D.A., Massoth G.J., McDuff R.E., Lupton J.E., Lilley M.D., 1990. Geochemistry of hydrothermal fluids from Axial Seamount hydrothermal emissions study vent field, Juan de Fuca Ridge: Subseafloor boiling and subsequent fluid-rock interaction. Journal of Geophysical Research 95, 12895.

Cathles L.M., 1983. An Analysis of the Hydrothermal System Responsible for Massive Sulfide Deposition in the Hokuroku Basin of Japan. Economic Geology Monograph Series 5, 439-487.

Chakrabarti R., Basu A.R., Bandyopadhyay P.K., Zou H., 2011. Age and Origin of the Chilka Anorthosites, Eastern Ghats, India: Implications for Massif Anorthosite Petrogenesis and Break-up of Rodinia. Springer EBooks, 355-382.

Clayton R.N., O'Neil J.R., Mayeda T.K., 1972. Oxygen isotope exchange between quartz and water. Journal of Geophysical Research 77, 3057-3067.

Cooke D.R., Bull S.W., Large R.R., McGoldrick P.J., 2000. The Importance of Oxidized Brines for the Formation of Australian Proterozoic Stratiform Sediment-Hosted Pb-Zn (Sedex) Deposits. Economic Geology 95, 1-18.

Cumming G.L. and Richards J.R., 1975. Ore lead isotope ratios in a continuously changing earth. Earth and Planetary Science Letters 28, 155-171.

Çağatay A., Pehlivanoğlu H., Altun Y., 1980. Küre piritli bakır yataklarının kobalt-altın mineralleri ve yatakların bu metaller açısından ekonomik değeri. Bulletin of the Mineral Research and Exploration 93-94, 110-117.

Çağatay M.N., 1993. Hydrothermal alteration associated with volcanogenic massive sulfide deposits; examples from Turkey. Economic Geology 88, 606-621.

Çakır Ü., 1995. Aşıköy Toykondu (Küre-Kastamonu) Masif Sülfid Yataklarının Jeolojik Özellikleri. Maden Tetkik ve Arama Dergisi 117, 29-40.

Çavdar B. and Günay K., 2023. Soil geochemistry prospection of a mafic-clastic type volcanogenic massive sulfide deposit in Central Pontides: a case study from the Sarıseki deposit (Kastamonu, Türkiye). Neues Jahrbuch Für Mineralogie - Abhandlungen 198, 211-233.

Çavdar B. and Günay K., 2025. Soil geochemistry characteristics of bimodal-mafic type VMS deposits in the Central Pontides: Importance of data investigation in exploration and following discovery. Turkish Journal of Earth Sciences 34, 504-531.

Çavdar B., Günay K., Baran C., Coşkun K., Sözcü A., Ersoy G.G., Dönmez C., Özkümüş S., Cingil E.O., 2024. Orta Karadeniz Bölgesi'ndeki metalik maden arama çalışmaları. MTA Doğal Kaynaklar ve Ekonomi Bülteni 38, 29-38.

Çavdar B., Günay K., Mutlu H., 2025a. Stream sediment and soil geochemistry of the largest volcanogenic massive sulfide deposit in Türkiye, Karaburun deposit (Central Pontides). Journal of Geochemical Exploration 277, 107816.

Çavdar B., Günay K., Oyan V., Mutlu H., Dönmez C., Çiftçi E., Tessalina S., 2025b. Geology, Geochemistry, and Geochronology of the Giant Pelitic-Mafic Type Karaburun Volcanogenic Massive Sulfide Deposit (Central Pontides, Turkey). Economic Geology 120, 1649-1677.

Çelik Ö.F., Chiaradia M., Marzoli A., Özkan M., Billor Z., Topuz G., 2016. Jurassic metabasic rocks in the Kızılırmak accretionary complex (Kargı region, Central Pontides, Northern Turkey). Tectonophysics 672-673, 34-49.

Çiftçi E. and Hagni R.D., 2005. Mineralogy of the Lahanos Deposit a Kuroko-Type Volcanogenic Massive Sulfide Deposit from the Eastern Pontides (Giresun-NE Turkey). Türkiye Jeoloji Bülteni/Geological Bulletin of Turkey 48, 55-64.

Çiftçi E. and Lermi A., 2014. Mineralogy and geochemistry of Taurides' Pb-Zn mineralization (Southern Turkey). 21st General Meeting of IMA South Africa 2014. Economic Geology/Mineralogy - Abstract and Poster Presentation.

Çiftçi E., 2019. Volcanogenic Massive Sulfide (VMS) Deposits of Turkey. In F. Pirajno, T. Ünlü, C. Dönmez and M. B. Şahin

(Eds.), Mineral Resources of Turkey. Modern Approaches in Solid Earth Sciences.

Çimen O., 2020a. Geochemical characteristics of a pre-Middle Jurassic oceanic crust fragment from the Central Pontides in northern Turkey: Geodynamic implications on intra-oceanic subduction initiation. Geochemistry 80, 125535.

Çimen O., 2020b. Geochemical characteristics of the adakite-like Dodurga Pluton (Central Pontides, N Turkey): implications for Middle Triassic continental arc magmatism in southern Black Sea region. International Journal of Earth Sciences 109, 809-829.

Çimen O., Göncüoğlu M.C., Sayıt K., 2016. Geochemistry of the metavolcanic rocks from the Çangaldağ Complex in the Central Pontides: implications for the Middle Jurassic arc-back-arc system in the Neotethyan Intra-Pontide Ocean. Turkish Journal of Earth Sciences 25, 491-512.

Çimen O., Göncüoğlu M.C., Simonetti A., Sayıt K., 2017. Whole rock geochemistry, Zircon U-Pb and Hf isotope systematics of the Çangaldağ Pluton: Evidences for Middle Jurassic Continental Arc Magmatism in the Central Pontides, Turkey. Lithos 290-291, 136-155.

Çimen O., Göncüoğlu M.C., Simonetti A., Sayıt K., 2018. New zircon U-Pb LA-ICP-MS ages and Hf isotope data from the Central Pontides (Turkey): Geological and geodynamic constraints. Journal of Geodynamics 116, 23-36.

Çimen O., Gücer M.A., Akal C., Göncüoğlu M.C., Arslan M., Simonetti A., Karaoğlan F., 2024. Revisiting the depositional age and provenance characteristics of metasedimentary rocks from the basement units in the Central Pontides (N Turkey): New constraints for tectonic evolution of the southern Black Sea region. Journal of Asian Earth Sciences 266, 106134.

de Ronde C.E.J., Channer D.M. de R., Faure K., Bray C.J., Spooner E.T.C., 1997. Fluid chemistry of Archean seafloor hydrothermal vents: Implications for the composition of circa 3.2 Ga seawater. Geochimica et Cosmochimica Acta 61, 4025-4042.

Deng J., Yang L.-Q., Groves D.I., Zhang L., Qiu K.-F., Wang Q.-F., 2020. An integrated mineral system model for the gold deposits of the giant Jiaodong province, eastern China. Earth-Science Reviews 208, 103274.

Doyle M.G. and Allen R.L., 2003. Subsea-floor replacement in volcanic-hosted massive sulfide deposits. Ore Geology Reviews 23(3-4), 183-222.

Dönmez C., Keskin S., Günay K., Çolakoğlu A., Çiftçi Y., Uysal İ., Türkel A., Yıldırım N., 2014. Chromite and PGE geochemistry of the Elekdağ Ophiolite (Kastamonu, Northern Turkey): Implications for deep magmatic processes in a supra-subduction zone setting. Ore Geology Reviews 57, 216-228.

Driesner T. and Heinrich C.A., 2007. The system H_2O-NaCl. Part I: Correlation formulae for phase relations in temperature-pressure-composition space from 0 to 1000 °C, 0 to 5000 bar, and 0 to 1 XNaCl. Geochimica et Cosmochimica Acta 71, 4880-4901.

Eldridge C.S., Barton P.B., Ohmoto H., 1983. Mineral Textures and Their Bearing on Formation of the Kuroko Orebodies. The Kuroko and Related Volcanogenic Massive Sulfide Deposits 5.

Eyüboğlu Y., Santosh M., Yi K., Tüysüz N., Korkmaz S., Akaryalı E., Dudas F.O., Bektaş O., 2014. The Eastern Black Sea-type volcanogenic massive sulfide deposits: Geochemistry, zircon U-Pb geochronology and an overview of the geodynamics of ore genesis. Ore Geology Reviews 59, 29-54.

Fakhri-Doodoui A. and Alipour-Asll M., 2024. Geology, geochemistry, mineralization and fluid inclusion characteristics of the SW of Hormuz Island banded iron formations, southern Iran. Geochemistry: Exploration, Environment, Analysis 24(1). doi: 10.1144/geochem2023-002

Franklin J.M., Gibson H.L., Galley A.G., Jonasson I.R., 2005. Volcanogenic massive sulfide deposits. Economic Geology 100th Anniversary Volume, 523-560.

Franklin J.M., Sangster D.M., Lydon, J.W., 1981. Volcanic-associated massive sulfide deposits. Economic Geology 75th Anniversary Volume, 485-627.

Frassi C., Marroni M., Pandolfi L., Göncüoğlu M.C., Ellero A., Ottria G., Sayıt K., McDonald C.S., Balestrieri M.L., Malasoma A., 2017. Burial and exhumation history of the Daday Unit (Central Pontides, Turkey): implications for the closure of the Intra-Pontide oceanic basin. Geological Magazine 155, 356-376.

Galley A.G., 1993. Characteristics of semi-conformable alteration zones associated with volcanogenic massive sulphide districts. Journal of Geochemical Exploration 48, 175-200.

Galley A.G., 2003. Composite synvolcanic intrusions associated with Precambrian VMS-related hydrothermal systems. Mineralium Deposita 38, 443-473.

Galley A.G., Hannington M.D., Jonasson I.R., 2007. Volcanogenic massive sulphide deposits. In W. D. Goodfellow (Ed.), Mineral Deposits of Canada: A Synthesis of Major Deposit-Types, District Metallogeny, the Evolution of Geological Provinces, and Exploration Methods. Geological Association of Canada, Mineral Deposits Division, 141-161.

Gardner H.D. and Hutcheon I., 1985. Geochemistry, mineralogy, and geology of the Jason Pb-Zn deposits, Macmillan Pass, Yukon, Canada. Economic Geology 80, 1257-1276.

Gemmell J.B., Sharpe R., Jonasson I.R., Herzig P.M., 2004. Sulfur Isotope Evidence for Magmatic Contributions to Submarine and Subaerial Gold Mineralization: Conical Seamount and the Ladolam Gold Deposit, Papua New Guinea. Economic Geology and the Bulletin of the Society of Economic Geologists 99, 1711-1725.

Gill S.B., Piercey S.J., Layne G.D., Piercey G., 2019. Sulphur and lead isotope geochemistry of sulphide minerals from the Zn-Pb-Cu-Ag-Au Lemarchant volcanogenic massive sulphide (VMS) deposit, Newfoundland, Canada. Ore Geology Reviews 104, 422-435.

Goldstein R.H. and Reynolds T.J., 1994. Systematics of Fluid Inclusions in Diagenetic Minerals. SEPM Society for Sedimentary Geology.

Goodfellow W.D. and McCutcheon S.R., 2003. Geologic and Genetic Attributes of Volcanic Sediment-Hosted Massive Sulfide Deposits of the Bathurst Mining Camp, Northern New Brunswick-A Synthesis. Economic Geology Monograph 11, 245-301.

Grossman E.L., 1998. Oxygen isotopes. Geochemistry.

Gökçe A. and Bozkaya G., 2007. Lead and sulfur isotopic studies of the barite-galena deposits in the Karalar area (Gazipaşa-Antalya), Southern Turkey. Journal of Asian Earth Sciences 30, 53-62.

Göncüoğlu M.C., Marroni M., Pandolfi L., Ellero A., Ottria G., Catanzariti R., Tekin U.K., Sayıt K., 2014. The Arkot Dağ Mélange in Araç area, central Turkey: Evidence of its origin within the geodynamic evolution of the Intra-Pontide suture zone. Journal of Asian Earth Sciences 85, 117-139.

Gücer M.A., Arslan M., Sherlock S., Heaman L.M., 2016. Permo-Carboniferous granitoids with Jurassic high temperature metamorphism in Central Pontides, Northern Turkey. Mineralogy and Petrology 110, 943-964.

Gücer M.A., Arslan M., Çimen O., Sherlock S.C., 2019. Petrology and 40Ar-39Ar dating of paragneisses from the Devrekani Massif (Central Pontides, Northern Turkey): Implications for the Jurassic high-T metamorphism in an extensional tectonic environment. Journal of Asian Earth Sciences 181, 103888.

Günay K., 2021. Geological and geochemical characteristics of the Cünür volcanogenic massive sulfide mineralization (Kastamonu, Turkey). Bulletin of the Mineral Research and Exploration 165, 77-96.

Günay K., 2023. Geological, geochemical and geochronological characteristics of the Büyük Hill bimodal-mafic type volcanogenic massive sulfide deposit (Central Pontides, Türkiye): Implications for an island arc tectonic setting. Neues Jahrbuch für Mineralogie - Abhandlungen 198, 191-210.

Günay K., Dönmez C., Uysal İ., Yıldırım N., Şahin M.B., Yıldırım E., Tablacı A., Kang J., Lee I., 2016. Chrome spinel geochemistry of ultramafic rocks from the Elekdağ metaophiolite (Northern Turkey): Implications for greenschist to mid-amphibolite facies metamorphism. Neues Jahrbuch für Mineralogie - Abhandlungen 193, 215-230.

Günay K., Dönmez C., Oyan V., Yıldırım N., Çiftçi E., Yıldız H., Özkümüş S., 2018. Geology and geochemistry of sediment-hosted Hanönü massive sulfide deposit (Kastamonu, Turkey). Ore Geology Reviews 101, 652-674.

Günay K., Dönmez C., Oyan V., Baran C., Çiftçi E., Parlak O., Yıldırım N., Deng X.-H., Li C., Yıldırım E., Özkümüş S., 2019. Geology, geochemistry and Re-Os geochronology of the Jurassic Zeybek volcanogenic massive sulfide deposit (Central Pontides, Turkey). Ore Geology Reviews 111, 102994.

Günay K., Oyan V., Dönmez C., Çavdar B., Çiftçi E., Chugaev A.V., Yıldırım N., Parlak O., Yıldırım E., Wang L.X., Ma C.Q., 2022. Au-rich bimodal-mafic type volcanogenic massive sulphide deposit associated with Jurassic arc volcanism from the Central Pontides (Kastamonu, Turkey). Ore Geology Reviews 141, 104660.

Günay K. and Çavdar B., 2024. Orta Karadeniz masif sülfid yataklarının tektonomagmatik oluşum ortamları. MTA Doğal Kaynaklar ve Ekonomi Bülteni 37, 1-10. (in Turkish)

Günay K., Çavdar B., Coşkun K., Ersoy G.G., Yas T., Baran C., Cingil E.O., 2024. Sinop İli Boyabat İlçesi Karaburun S:202101691 (Er: 3416434) No'lu IV. Grup Ruhsatına Ait Bakır Sahasının UMREK Koduna Uygun Maden Jeolojisi ve Kaynak Tahmin Raporu. MTA Genel Müdürlüğü, Ankara. Unpublished report (in Turkish).

Güner M., 1980. Küre Civarının Masif Sülfit Yatakları ve Jeolojisi, Pontidler (Kuzey Türkiye). Bulletin of the Mineral Research and Exploration 93-94, 65-109.

Hannington M.D., Jonasson I.R., Herzig P.M., Petersen S., 1995. Physical and Chemical Processes of Seafloor Mineralization at Mid-Ocean Ridges. In Seafloor Hydrothermal Systems: Physical, Chemical, Biological, and Geological Interactions (Eds. S.E. Humphris, R.A. Zierenberg, L.S. Mullineaux and R.E. Thomson). doi: 10.1029/GM091p0115

Herzig P.M. and Hannington M.D., 1995. Polymetallic massive sulfides at the modern seafloor a review. Ore Geology Reviews 10(2), 95-115.

Hoefs J., 1984. Stable Isotope Geochemistry. (3rd ed.). Springer.

Hoefs J., 2009. Stable Isotope Geochemistry. (6th ed.). Springer.

Hoefs J., 2021. Stable Isotope Geochemistry (9th ed.). Springer.

Hou Z., Khin Z., Peter R., Li Y., Qu X., Song S., Peng L., Huang J. 2008. Geology, Fluid Inclusions, and Oxygen Isotope Geochemistry of the Baiyinchang Pipe-Style Volcanic-Hosted Massive Sulfide Cu Deposit in Gansu Province, Northwestern China. Economic Geology 103, 269-292.

Hurai V., 2010. Fluid inclusion geobarometry: Pressure corrections for immiscible H_2O-CH_4 and H_2O-CO_2 fluids. Chemical Geology 278(3-4), 201-211.

Huston D.L. and Champion D.C., 2023. Applications of Lead Isotopes to Ore Geology, Metallogenesis and Exploration. In: Huston, D., Gutzmer, J. (Eds.) Isotopes in Economic Geology, Metallogenesis and Exploration. Mineral Resource Reviews, 155-187.

Huston D.L., 1999. Stable Isotopes and Their Significance for Understanding the Genesis of Volcanic-Hosted Massive Sulfide Deposits: A Review. Reviews in Economic Geology 10, 151-180.

Huston D.L., Laflamme C., Beaudoin G., Piercey S., 2023. Light Stable Isotopes in Volcanic-Hosted Massive Sulfide Ore Systems. Mineral Resource Reviews, 245-282.

Huston D.L., Relvas J.M.R.S., Gemmell J.B., Drieberg S., 2011. The role of granites in volcanic-hosted massive sulphide ore-forming systems: an assessment of magmatic-hydrothermal contributions. Mineralium Deposita 46(5-6), 473-507.

İmer A., Richards J.P., Muehlenbachs K., 2016. Hydrothermal Evolution of the Çöpler Porphyry-Epithermal Au Deposit, Erzincan Province, Central Eastern Turkey. Economic Geology 111, 1619-1658.

Kahya A. and Kuşcu E., 2022. S and Pb isotope characteristics and fluid inclusions of the metamorphic rock hosted massive sulfide mineralization at the village of Başçatak (Yozgat province, Turkey) in the Central Anatolian Crystalline Complex. Neues Jahrbuch Für Mineralogie - Abhandlungen Journal of Mineralogy and Geochemistry 198, 85-99.

Kaya M., Kumral M., Yalçın C., Abdelnasser A., 2023. Sulfur and Carbon-Oxygen Isotopic Geochemistry and Fluid Inclusion Characteristics of the Yolindi Cu-Fe Skarn Mineralization, Biga Peninsula, NW Turkey: Implications for the Source and Evolution of Hydrothermal Fluids. Minerals 13, 1542.

Kesler S.E., 2005. Ore-Forming Fluids. Elements 1, 13-18.

Kiss G.B., Garuti G., Zaccarini F., 2015. Fluid inclusion study of the Boccassuolo VMS-related stockwork deposit (Northern-Apennine ophiolites, Italy). Geologia Croatica 68, 285-302.

Knauth L. and Roberts S.K., 1991. The hydrogen and oxygen isotope history of the Silurian-Permian hydrosphere as determined by direct measurements of fossil water. Stable Isotope Geochemistry: A Tribute to Samuel Epstein, 91-104.

Koç Ş., Ünsal A., Kadıoğlu Y.K., 1995. Küre (Kastamonu) Cevherleşmelerini İçeren Volkanitlerin Jeolojisi, Jeokimyası ve Jeotektonik Konumu. MTA Dergisi 117, 41-54.

Kozur H.W., Aydın M., Demir O., Yakar H., Göncüoğlu M.C., Kuru F., 2000. New Stratigraphic and Palaeogeographic Results from the Palaeozoic and Early Mesozoic of the Middle Pontides (Northern Turkey) in the Azdavay, Devrekani, Kre and Inebolu Areas: Implications for the Carboniferous - Early Cretaceous Geodynamic Evolution an. Geologia Croatica 53(2), 209-268.

Köprübaşı N., Çiftçi E., Cordan S., Köprübaşı N., Özkul C., Şişman Tükel F., 2014. Comparative geochemical study of soils developed on characteristic black and yellow polymetallic massive sulfide deposits in Eastern Pontides (NE Turkey). Turkish Journal of Earth Sciences 23, 129-146.

Kuşcu İ. and Erler A., 2002. Pyrite Deformation Textures in the Deposits of the Küre Mining District (Kastamonu-Turkey). Turkish Journal of Earth Sciences 11, 205-215.

Kuşcu İ., Tosdal R.M., Gençalioğlu-Kuşcu G., 2019. Episodic porphyry Cu (-Mo-Au) formation and associated magmatic evolution in Turkish Tethyan collage. Ore Geology Reviews 107, 119-154.

Leach D.L., Sangster D.F., Kelley K.D., Large R.R., Garven G., Allen C.R., Gutzmer J., Walters S., 2005. Sediment-Hosted Lead-Zinc DepositsA Global Perspective. One Hundredth Anniversary Volume.

Lecumberri-Sanchez P., Steele-MacInnis M., Bodnar R.J., 2012. A numerical model to estimate trapping conditions of fluid inclusions that homogenize by halite disappearance. Geochimica et Cosmochimica Acta 92, 14-22.

Lentz D. R., 1998. Petrogenetic evolution of felsic volcanic sequences associated with Phanerozoic volcanic-hosted massive sulphide systems: the role of extensional geodynamics. Ore Geology Reviews 12, 289-327.

Lydon J.W., 1988. Ore Deposit Models #14. Volcanogenic Massive Sulphide Deposits Part 2: Genetic Models. Geoscience Canada 15, 43-65.

Maghfouri S., Rastad E., Lentz D.R., Mousivand F., Choulet F., 2018. Mineralogy, microchemistry and fluid inclusion studies of the Besshi-type Nudeh Cu-Zn VMS deposit, Iran. Geochemistry 78, 40-57.

Mao Q., Wang J., Xiao W., Windley B.F., Schulmann K., Yu M. H., Fang T., Li Y., 2018. Mineralization of an intra-oceanic arc in an accretionary orogen: Insights from the Early Silurian Honghai volcanogenic massive sulfide Cu-Zn deposit and associated adakites of the Eastern Tianshan (NW China). Geological Society of America Bulletin 131(5-6), 803-830.

Marroni M., Frassi C., Göncüoğlu M.C., Vincenzo G.D., Pandolfi L., Rebay G., Ellero A., Ottria G., 2014. Late Jurassic amphibolite-facies metamorphism in the Intra-Pontide Suture Zone (Turkey): an eastward extension of the Vardar Ocean from the Balkans into Anatolia? Journal of the Geological Society 171, 605-608.

Marroni M., Göncüoğlu M.C., Frassi C., Sayıt K., Pandolfi L., Ellero A., Ottria G., 2020. The Intra-Pontide ophiolites in Northern Turkey revisited: From birth to death of a Neotethyan oceanic domain. Geoscience Frontiers 11, 129-149.

Misra K.C., 2000. Understanding mineral deposits. Kluwer.

Monecke T., Petersen S., Hannington M.D., 2014. Constraints on Water Depth of Massive Sulfide Formation: Evidence from Modern Seafloor Hydrothermal Systems in Arc-Related Settings. Economic Geology 109, 2079-2101.

Mosier D.L., Berger V.I., Singer D.A., 2009. Volcanogenic massive sulfide deposits of the world: Database and grade and tonnage models. U.S. Geological Survey, 1-46.

Ohmoto H., 1972. Systematics of Sulfur and Carbon Isotopes in Hydrothermal Ore Deposits. Economic Geology 67, 551-578.

Ohmoto H., 1996. Formation of volcanogenic massive sulfide deposits: The Kuroko perspective. Ore Geology Reviews 10(3-6), 135-177.

Okay A.İ. and Nikishin A.M., 2015. Tectonic evolution of the southern margin of Laurasia in the Black Sea region. International Geology Review 57(5-8), 1051-1076.

Okay A.İ. and Tüysüz O., 1999. Tethyan sutures of northern Turkey. In B. Durand, L. Jolivet, F. Horvath and M. Seranne (Eds.), The Mediterranean Basins: Tertiary Extension within the Alpine Orogen. Geological Society, London, Special Publications 156, 475-515.

Okay A.İ., Altıner D., Sunal G., Aygül M., Akdoğan R., Altiner S., Simmons M., 2018. Geological evolution of the Central Pontides. Geological Society, London, Special Publications 464, 33-67.

Okay A.İ., Sunal G., Sherlock S., Altıner D., Tüysüz O., Kylander-Clark A.R.C., Aygül M., 2013. Early Cretaceous sedimentation and orogeny on the active margin of Eurasia: Southern Central Pontides, Turkey. Tectonics 32, 1247-1271.

Okay A.İ., Sunal G., Tüysüz O., Sherlock S., Keskin M., Kylander-Clark A.R.C., 2014. Low-pressure-high-temperature metamorphism during extension in a Jurassic magmatic arc, Central Pontides, Turkey. Journal of Metamorphic Geology 32, 49-69.

Okay A.İ., Tüysüz O., Satir M., Özkan-Altıner S., Altıner D., Sherlock S., Eren R.H., 2006. Cretaceous and Triassic subduction-accretion, high-pressure-low-temperature metamorphism, and continental growth in the Central Pontides, Turkey. Geological Society of America Bulletin 118(9-10), 1247-1269.

Özkan B., Sarı R., Terzioğlu Y., Çimen O., 2025. Discovery of the buried Örhen VMS Cu-Zn±Au Deposit (Central Pontides, Türkiye): Preliminary geological and geochemical findings. 77. Türkiye Jeoloji Kurultayı Bildiri Özleri Kitabı 157, 563.

Peter J.M. and Scott S.D., 1999. Windy Craggy, Northwestern British Columbia: The World's Largest Besshi-Type Deposit. In C. T. Barrie and M. D. Hannington (Eds.), Volcanic Associated Massive Sulfide Deposits: Processes and Examples in Modern and Ancient Settings. Reviews in Economic Geology 8, 261-295.

Piercey S.J., 2011. The setting, style, and role of magmatism in the formation of volcanogenic massive sulfide deposits. Mineralium Deposita 46(5-6), 449-471.

Piercey S.J., Mortensen J.K., Creaser R.A., 2003. Neodymium isotope geochemistry of felsic volcanic and intrusive rocks from the Yukon-Tanana Terrane in the Finlayson Lake Region, Yukon, Canada. Canadian Journal of Earth Sciences 40, 77-97.

Pirajno F., 2009. Hydrothermal processes and mineral systems. Springer, 1250.

Potter I.I., 1976. Pressure corrections for fluid-inclusion homogenization temperatures based on the volumetric properties of the system NaCl-H_2O. Journal of Research of the U. S. Geological Survey 5, 603-607.

Rabayrol F., Wainwright A.J., Lee R.G., Hart C.J.R., Creaser R.A., Camacho A., 2023. District-Scale VMS to Porphyry-Epithermal Transitions in Subduction to Post collisional Tectonic Environments: The Artvin Au-Cu District and the Hod Gold Corridor, Eastern Pontides Belt, Turkey. Economic Geology 118, 801-822.

Revan M.K., Genç Y., Maslennikov V.V., Ünlü T., Delibaş O., Hamzaçebi S. 2013. Doğu Karadeniz Bölgesi (KD Türkiye) Volkanojenik Masif Sülfid Yatakları Cevher Fasiyeslerine Ait Bazı Özgün Bulgular. Maden Tetkik ve Arama Dergisi 147, 73-90.

Revan M.K., Hisatani K., Miyamoto H., Delibaş O., Hanilçi N., Aysal N., Özkan M., Çolak T., Karslı Ş., Peytcheva I. 2017. Geology, U-Pb geochronology, and stable isotope geochemistry of the Tunca semi-massive sulfide mineralization, Black Sea region, NE Turkey: Implications for ore genesis. Ore Geology Reviews 89, 369-389.

Richards J.P., 2015. Tectonic, magmatic, and metallogenic evolution of the Tethyan orogen: From subduction to collision. Ore Geology Reviews 70, 323-345.

Roedder E. and Bodnar R.J., 1980. Geologic Pressure Determinations from Fluid Inclusion Studies. Annual Review of Earth and Planetary Sciences 8, 263-301.

Roedder E., 1984. Fluid inclusions. Reviews in Mineralogy 12.

Rollinson H. and Pease V. 2021. Using Geochemical Data to Understand Geological Processes (2nd ed.). Cambridge University Press.

Rye R.O., 1993. The evolution of magmatic fluids in the epithermal environment; the stable isotope perspective. Economic Geology 88, 733-752.

Sangster D.F., 2002. The role of dense brines in the formation of vent-distal sedimentary-exhalative (SEDEX) lead-zinc deposits: field and laboratory evidence. Mineralium Deposita 37, 149-157.

Sato K. and Sasaki A., 1980. Lead isotopic feature of the Besshi-type deposits and its bearing on the ore lead evolution. Geochemical Journal 14, 303-315.

Sato K., Delevaux M.H., Doe B.R., 1981. Lead isotope measurements on ores, igneous and sedimentary rocks from the kuroko mineralization area. Geochemical Journal 15, 135-140.

Sayıt K., Marroni M., Göncüoğlu M.C., Pandolfi L., Ellero A., Ottria G., Frassi C., 2016. Geological setting and geochemical signatures of the mafic rocks from the Intra-Pontide Suture Zone: implications for the geodynamic reconstruction of the Mesozoic Neotethys. International Journal of Earth Sciences 105, 39-64.

Seal R.R., 2006. Sulfur Isotope Geochemistry of Sulfide Minerals. Reviews in Mineralogy and Geochemistry 61, 633-677.

Shanks III W.C., 2001. Stable Isotopes in Seafloor Hydrothermal Systems: Vent fluids, hydrothermal deposits, hydrothermal alteration, and microbial processes. Reviews in Mineralogy and Geochemistry 43, 469-525.

Sharp Z.D. and Kirschner D.L., 1994. Quartz-calcite oxygen isotope thermometry: A calibration based on natural isotopic variations. Geochimica et Cosmochimica Acta 58, 4491-4501.

Shepherd T., Rankın A.H., Alderton D.H.M., 1985. A pracitcal guide to fluid inclusion studies. Blackie, 1-239.

Sheppard S.M.F., 1981. Stable isotope geochemistry of fluids. Physics and Chemistry of the Earth 13-14, 419-445.

Sheppard S., 1986. Characterization and isotopic variations in natural waters. Reviews in Mineralogy & Geochemistry 16, 165-183.

Slack J.F., 1993. Descriptive and grade-tonnage models for Besshi-type massive sulphide deposits. Geological Association of Canada, Special Paper 40, 343-371.

Slack J.F., Shanks W.C., Woodruff L.G., 2024. Seeing

Through Metamorphism: Geochemical and Isotopic Studies of Amphibolite Facies Mafic-Siliciclastic (Besshi-Type) Massive Sulfide Deposits at the Elizabeth Copper Mine, Vermont, USA. Economic Geology 119, 1487-1524.

Solomon M., Tornos F., Large R.R., Badham J.N.P., Both R.A., Zaw K. 2004. Zn-Pb-Cu volcanic-hosted massive sulphide deposits: criteria for distinguishing brine pool - from black smoker-type sulphide deposition. Ore Geology Reviews 25, 259-284.

Sönmez Ş.U., Moritz R., Keskin S., Bilir M.E., Turlin F., Ulianov A., Spikings R., Kouzmanov K., Putlitz B., Vennemann T., Aydın Ü., 2025. Late Cretaceous magmatic controls on epithermal-porphyry and volcanogenic massive sulfide systems in the Eastern Pontides, Northeast Türkiye: geochemical and geochronological evidence. Mineralium Deposita.

Stacey J.S. and Kramers J.D., 1975. Approximation of terrestrial lead isotope evolution by two-stage model. Earth and Planetary Science Letters 26, 207-221.

Steele-MacInnis M., Lecumberri-Sanchez P., Bodnar R.J., 2012. HokieFlincs_H_2O-NaCl : A Microsoft Excel spreadsheet for interpreting microthermometric data from fluid inclusions based on the PVTX properties of H_2O-NaCl. Computers & Geosciences 49, 334-337.

Şengör A.M.C. and Yılmaz Y., 1981. Tethyan evolution of Turkey: A plate tectonic approach. Tectonophysics 75(3-4), 181-241.

Taylor B.E., 1987. Stable isotope geochemistry of ore forming fluids. Mineralogical Association of Canada, Short Course Series 13, 337-445.

Taylor H.P., 1974. The Application of Oxygen and Hydrogen Isotope Studies to Problems of Hydrothermal Alteration and Ore Deposition. Economic Geology 69, 843-883.

Tekin U.K., Göncüoğlu M.C., Pandolfi L., Marroni M., 2012. Middle-Late Triassic radiolarian cherts from the Arkotdağ mélange in northern Turkey: implications for the life span of the northern Neotethyan branch. Geodinamica Acta 25(3-4), 305-319.

Tessalina S.G., Herrington R.J., Taylor R.N., Sundblad K., Maslennikov V.V., Orgeval J.J., 2016. Lead isotopic systematics of massive sulphide deposits in the Urals: Applications for geodynamic setting and metal sources. Ore Geology Reviews 72, 22-36.

Tornos F. and Chiaradia M., 2004. Plumbotectonic Evolution of the Ossa Morena Zone, Iberian Peninsula:Tracing the Influence of Mantle-Crust Interaction in Ore-Forming Processes. Economic Geology 99, 965-985.

Tornos F., Peter J.M., Allen R., Conde C., 2015. Controls on the siting and style of volcanogenic massive sulphide deposits. Ore Geology Reviews 68, 142-163.

Tüysüz O., 1999. Geology of the Cretaceous sedimentary basins of the Western Pontides. Geological Journal 34(1-2), 75-93.

Unruh D.M., Fey D.L., Church S.E., 2000. Chemical Data and Lead İsotopic Compositions of Geochemical Baseline Samples from Streambed Sediments and Smelter Slag, Lead İsotopic Compositions in Fluvial Tailings, and Dendrochronology Results from the Boulder River Watershed, Jefferson County, Montana. U.S. Geological Survey.

Ustaömer T. and Robertson A.H.F., 1993. A Late Palaeozoic-Early Mesozoic marginal basin along the actives sourthern continental margin of Eurasia: Evidence from the central Pontides (Turkey) and adjacent regions. Geological Journal 28(3-4), 219-238.

Ustaömer T. and Robertson A.H.F., 1994. Late Palaeozoic marginal basin and subduction-accretion: the Palaeotethyan Küre Complex, Central Pontides, northern Turkey. Journal of Geological Society, London 151, 291-305.

Ustaömer T. and Robertson A.H.F., 1999. Geochemical evidence used to test alternative plate tectonic models for pre-Upper Jurassic (Palaeotethyan) units in the Central Pontides, N Turkey. Geological Journal 34(1-2), 25-53.

Vanko D.A., Bach W., Roberts S., Yeats C.J., Scott S.D., 2004. Fluid inclusion evidence for subsurface phase separation and variable fluid mixing regimes beneath the deep-sea PACMANUS hydrothermal field, Manus Basin back arc rift, Papua New Guinea. Journal of Geophysical Research 109(B3).

Wilkinson J.J., 2001. Fluid inclusions in hydrothermal ore deposits. Lithos 55(1-4), 229-272.

Wilkinson J.J., 2010. A Review of Fluid Inclusion Constraints on Mineralization in the Irish Ore Field and Implications for the Genesis of Sediment-Hosted Zn-Pb Deposits. Economic Geology 105, 417-442.

Wilkinson J.J., Stoffell B., Wilkinson C.C., Jeffries T.E., Appold M.S., 2009. Anomalously Metal-Rich Fluids Form Hydrothermal Ore Deposits. Science 323(5915), 764-767.

Yalçın C., Hanilçi N., Kumral M., Kaya M., 2022. Magnetite geochemistry of Beshhi-type Cu-Zn mineralizations in Central Pontides (Kargı-Çorum). 2nd Advanced Engineering Days, 30-32.

Yalçın C., Hanilçi N., Kumral M., Kaya M., 2023. Geological, geochemical and fluid inclusion features of Kömürlükdere and Göçükdibi Cu-Zn ore (Central Pontides, Turkey): Implications for their genesis. Geochemistry 83(4), 126005.

Yıldırım N., Dönmez C., Kang J., Lee I., Pirajno F., Yıldırım E., Günay K., Seo J.-H., Farquhar J. and Chang S.W., 2016. A magnetite-rich Cyprus-type VMS deposit in Ortaklar: A unique VMS style in the Tethyan metallogenic belt, Gaziantep, Turkey. Ore Geology Reviews 79, 425-442.

Yıldırım N., Eroğlu M., Dönmez C., Çetiner L., 2019. Malatya-Pötürge-Seyderesi Yöresindeki Ar:201901491 Er:3388626 Nolu IV. Grup Ruhsat Sahasına Ait Ag, Au, Cu ve Zn Madenlerinin Buluculuk Talebine Esas Kaynak Tahmin Raporu. MTA Genel Müdürlüğü, Ankara. Unpublished report. In Turkish.

Yiğit O., 2009. Mineral Deposits of Turkey in Relation to

Tethyan Metallogeny: Implications for Future Mineral Exploration. Economic Geology 104, 19-51.
Yu P.P., Zheng Y., Wang C.M., 2020. Trace elemental and sulfur-lead isotopic variations in metamorphosed volcanogenic massive sulfide (VMS) mineralization systems: An example from the Keketale Pb-Zn(-Ag) deposit, NW China. Ore Geology Reviews 125, 103685.
Zartman R.E. and Doe B.R., 1981. Plumbotectonics-the model. Tectonophysics 75(1-2), 135-162.
Zartman R.E. and Haines S.M., 1988. The plumbotectonic model for Pb isotopic systematics among major terrestrial reservoirs-A case for bi-directional transport. Geochimica et Cosmochimica Acta 52, 1327-1339.